Atmos. Chem. Phys. Discuss., 15, 2853–2904, 2015
www.atmos-chem-phys-discuss.net/15/2853/2015/
doi:10.5194/acpd-15-2853-2015

Atmospheric Chemistry and Physics Discussions

Observations of relative humidity effects on aerosol light scattering in the Yangtze River Delta of China

L. Zhang[1,2], J. Y. Sun[1,3], X. J. Shen[1], Y. M. Zhang[1], H. C. Che[1], Q. L. Ma[4], Y. W. Zhang[1], X. Y. Zhang[1], and J. A. Ogren[5]

[1]Key Laboratory of Atmospheric Chemistry of CMA, Institute of Atmospheric Composition, Chinese Academy of Meteorological Sciences, Beijing 100081, China
[2]College of Earth Science, University of Chinese Academy of Sciences, Beijing 100049, China
[3]State Key Laboratory of Cryospheric Sciences, Cold and Arid Region Environmental and Engineering Research Institute, Chinese Academy of Sciences, Lanzhou 730000, China
[4]LinAn Regional Atmosphere Background Station, LinAn 311307, China
[5]Earth System Research Laboratory, NOAA, Boulder, CO, USA

Received: 10 October 2014 – Accepted: 23 December 2014 – Published: 29 January 2015

Correspondence to: J. Y. Sun (jysun@cams.cma.gov.cn)

Published by Copernicus Publications on behalf of the European Geosciences Union.

Abstract

Scattering of solar radiation by aerosol particles is highly dependent on relative humidity (RH) as hygroscopic particles take up water with increasing RH. To achieve a better understanding of the effect of aerosol hygroscopic growth on light scattering properties and radiative forcing, a field campaign was carried out in the Yangtze River Delta of China in March 2013. During the observation period, the mean and standard deviation of enhancement factors at RH = 85 % for the scattering coefficient ($f(85\,\%)$), backscattering coefficient ($f_b(85\,\%)$) and hemispheric backscatter fraction ($f_\beta(85\,\%)$) were 1.58 ± 0.12, 1.25 ± 0.07 and 0.79 ± 0.04, respectively, i.e. aerosol scattering coefficient and backscattering coefficient increased by 58 and 25 % as the RH increased from 40 to 85 %. Meanwhile, the aerosol hemispheric backscatter fraction decreased by 21 %. The relative amount of organic matter (OM) and inorganics in PM_1 was found to be a main factor determining the magnitude of $f(RH)$, the highest values of $f(RH)$ corresponded to the aerosols with a small fraction of organic matter (OM), and vice versa. The relative amount of NO_3^- in fine particles was strongly correlated to $f(85\,\%)$, which suggests NO_3^- played a vital role in aerosol hygroscopic growth during this study. The mass percentage of nitrate also had a close relation to the curvature of humidograms, namely, the higher the nitrate concentration is, the straighter the humidogram will be. Air masses that arrived at LinAn in March can be classified into northerly-polluted, locally-polluted and dust-influenced types, the scattering enhancement factors at 85 % RH were 1.52 ± 0.10, 1.64 ± 0.09 and 1.48 ± 0.05, respectively. The sensitivity of the aerosol radiative forcing to $f(RH)$ at the measured mean ambient RH 67 % for various aerosol types was also estimated. The direct radiative forcing increased by 11.8, 19.5, and 10.5 %, respectively, for locally-polluted, northerly-polluted and dust-influenced aerosols due to aerosol hygroscopic growth at LinAn in March 2013.

ACPD
15, 2853–2904, 2015

1 Introduction

Hygroscopic aerosols take up water as humidity increases (Engelhart et al., 2011; Pilinis et al., 1989; Hänel, 1976; Covert et al., 1972). Aerosol water matters since water can affect both the size and refractive indices of atmospheric aerosols, thereby influencing the mass concentration, size distribution, and corresponding optical properties (e.g., scattering coefficient, backscattering coefficient, single scattering albedo, and asymmetry parameter) (Cheng et al., 2008; Randles et al., 2004; Malm et al., 2003; Carrico et al., 2003). In particular, understanding the effect of relative humidity on aerosol light scattering is important to better estimate the radiative forcing and evaluate visibility impairment (Ackerman et al., 2004; Tang, 1996; Charlson et al., 1992; Covert et al., 1972). Besides, most of the ground-based aerosol measurements are conducted in dry conditions so as to have a consistency within networks. These measurements can differ significantly from the ambient ones. Thus, the determination of enhancement factors for various optical variables are of crucial importance for climate forcing calculations (Quinn et al., 1995; Pilinis et al., 1995) and the comparison between remote sensing and ground based measurements (Zhang et al., 2012; Wang and Martin, 2007; Zieger et al., 2012).

The Yangtze River Delta, one of the most populated and fastest growing regions in China, has experienced extraordinary economic growth during the last two decades. Amounting to 2.1 % of the land area of China, this region contains ∼ 11 % of the country's population and produces ∼ 20 % of China's Gross Domestic Product (GDP) in 2013 (Wang et al., 2013). Concurrent with population increase and economic growth are the increasing energy consumption and growing number of automobiles, and therefore, the Yangtze River Delta has become a significant source of gas and particulate pollutants and secondary aerosol production. A 5-week field campaign was carried out in the early winter of 1999 at LinAn, a background station in the Yangtze River Delta (Xu et al., 2002). However, since then the physical and chemical properties of gas and particulate pollutants have changed dramatically with the rapidly developing economy

ACPD
15, 2853–2904, 2015

and fast growing population (Qi et al., 2012; Xu et al., 2008; Xia et al., 2007; Pan et al., 2010). In order to better understand the aerosol light scattering properties and their dependency on relative humidity in the Yangtze River Delta, both the scattering and backscattering coefficients under dry (RH < 30 %) conditions and controlled relative humidity were measured, along with the chemical composition and particle number size distribution.

The enhancement factors discussed in this work include scattering enhancement factor $f(\mathrm{RH},\lambda)$, enhancement factor for backscattering coefficient $f_{\mathrm{b}}(\mathrm{RH},\lambda)$ and enhancement factor for hemispheric backscatter fraction $f_{\beta}(\mathrm{RH},\lambda)$. The impact of relative humidity on the aerosol light scattering coefficient is defined as scattering enhancement factor $f(\mathrm{RH},\lambda)$:

$$f(\mathrm{RH},\lambda) = \sigma_{\mathrm{sp}}(\mathrm{RH},\lambda)/\sigma_{\mathrm{sp}}(\mathrm{dry},\lambda) \quad (1)$$

where $\sigma_{\mathrm{sp}}(\mathrm{dry},\lambda)$ and $\sigma_{\mathrm{sp}}(\mathrm{RH},\lambda)$ represent scattering coefficients at wavelength λ in dry conditions and at a defined higher relative humidity, respectively.

Likewise, the impact of relative humidity on aerosol backscattering coefficient can be described as enhancement factor for backscattering coefficient $f_{\mathrm{b}}(\mathrm{RH},\lambda)$:

$$f_{\mathrm{b}}(\mathrm{RH},\lambda) = \sigma_{\mathrm{bsp}}(\mathrm{RH},\lambda)/\sigma_{\mathrm{bsp}}(\mathrm{dry},\lambda) \quad (2)$$

where $\sigma_{\mathrm{bsp}}(\mathrm{dry},\lambda)$ and $\sigma_{\mathrm{bsp}}(\mathrm{RH},\lambda)$ represent backscattering coefficients at wavelength λ in dry conditions and at a defined relative humidity, respectively. $f(\mathrm{RH},\lambda)$ and $f_{\mathrm{b}}(\mathrm{RH},\lambda)$ are always greater than 1 after water uptake (Weingartner et al., 1995).

Hemispheric backscatter fraction (b) is closely related to the upscatter fraction ($\bar{\beta}$), the fraction of incident solar radiation scattered into space (Wiscombe and Grams, 1976). The impact of relative humidity on aerosol hemispheric backscatter fraction can be defined as enhancement factor for hemispheric backscatter fraction $f_{\beta}(\mathrm{RH},\lambda)$ (Adam et al., 2012):

$$f_{\beta}(\mathrm{RH},\lambda) = b(\mathrm{RH},\lambda)/b(\mathrm{dry},\lambda) \quad (3)$$

ACPD
15, 2853–2904, 2015

where $b(\mathrm{dry},\lambda)$ and $b(\mathrm{RH},\lambda)$ represent hemispheric backscatter fraction at wavelength λ in dry conditions and at the defined relative humidity. b is defined as the ratio of backscattering coefficient to scattering coefficient: $b = \sigma_{\mathrm{bsp}}/\sigma_{\mathrm{sp}}$. Thus, $f_\beta(\mathrm{RH},\lambda)$ can be rewritten as: $f_\beta(\mathrm{RH},\lambda) = f_{\mathrm{b}}(\mathrm{RH},\lambda)/f(\mathrm{RH},\lambda)$.

The wavelength dependence of scattering enhancement factor $f(\mathrm{RH},\lambda)$ varies with generalized aerosol types. Kotchenruther and Hobbs (1998) and Zieger et al. (2010, 2011) found no pronounced wavelength dependence of $f(\mathrm{RH},\lambda)$ for biomass burning aerosols and arctic aerosols, respectively; Zieger et al. (2013) found small variations ($< 5\,\%$) of $f(\mathrm{RH},\lambda)$ at 450, 550 and 700 nm for several European sites; Kotchenruther et al. (1999) and Magi and Hobbs (2003) reported significant wavelength dependence of $f(\mathrm{RH},\lambda)$ for urban/industrial aerosols off the east coast of the United States. In this study, the wavelength dependence of enhancement factors was also investigated. Except when specially mentioned, all the parameters discussed in this study are based on the measurements at 550 nm wavelength only.

2 Experimental sites and instrumentation

2.1 Site description

This study was carried out during an intensive field sampling period from 1 to 31 March 2013 at LinAn Regional Atmosphere background station, which is a WMO GAW regional station (30.3° N, 119.73° E, 138 m a.s.l.) located in the center of Yangtze River Delta, China (Fang et al., 2013) (as shown in Fig. 1). It is approximately 11 km north of the city of LinAn, with a population of 1.5 million. The site is ~ 50 km west of Hangzhou (capital of Zhejiang Province with a population of ~ 8.8 million) and ~ 210 km southwest of Shanghai (a mega-city with a population of ~ 20 million). LinAn station is on the top of a small hill, in an area primarily covered by bamboo forests and paddy rice fields, and represents the background conditions of the Yangtze River Delta. North of the station is a small village with ~ 200 inhabitants. In addition, there is an activated

ACPD
15, 2853–2904, 2015

charcoal factory ∼ 1.4 km north of LinAn station that uses bamboo wood as its source material (Qi et al., 2012). During the observation period, the prevailing winds were northeasterly (NE) and southwesterly (SW) with an average wind speed of ∼ 2.5 m s^{-1} (SD 1.4 m s^{-1}). 72 h back trajectories showed two contrasting air mass origins: (1) air masses from Northern China through long-distance transport and (2) air masses from southerly/southwesterly directions with a much shorter transport distance.

2.2 Measurement system and data processing

The scattering enhancement factor f(RH) is defined as the ratio of aerosol scattering coefficient at a given, elevated RH to that at a low RH (< 30 %). Correspondingly, the measurement system included two nephelometers operating in series with a humidifier between them. Sample air entered the first nephelometer (reference nephelometer or DryNeph) through an aerosol dryer (Shen et al., 2011; Tuch et al., 2009), where the sample RH was controlled to < 30 %, then passed through the humidifier, where the sample RH was regulated to a higher RH that was ramped from ∼ 40 to 90 %, and finally entered the second nephelometer (humidified nephelometer or WetNeph) where the scattering coefficient of humidified aerosols was measured.

Aerosol total scattering (between 7 and 170°) and backscattering coefficients (between 90 and 170°) were measured by an Integrating Nephelometer (TSI Inc., Model 3563) at three wavelengths: blue (450 nm), green (550 nm) and red (700 nm). Data were recorded as 1 min average and a zero check was performed automatically once per hour. The detailed information of this instrument has been described in many previous studies (Anderson and Ogren, 1998; Charlson et al., 1969; Anderson et al., 1996).

The humidifier was built by the aerosol group in Global Monitoring Division, Earth System Research Laboratory, National Ocean & Atmospheric Administration, USA (NOAA/GMD), which was described in Carrico et al. (1998). It consists of 2 concentric tubes with a heater and insulation around the outer tube. Sample air flows through the inner tube, while water circulates between the inner and outer tubes. The inner tube is made of porous extruded PTFE (polytetrafluoroethylene) membrane, whose pore size

ACPD
15, 2853–2904, 2015

is large enough for water molecules, but too small for larger molecules such as oxygen to cross. The flux of water vapor through the membrane is controlled by regulating the electric current to the humidifier heater until the desired RH is attained. The humidity scan was a 1 h cycle; RH was ramped from ~ 40 to 90 % during the first half hour and in the reverse direction during the last half hour.

Besides the scattering measurement, particle number size distribution and aerosol chemistry were also measured at the station. Particle number size distributions from 3 nm to 10 µm were measured by a twin differential mobility particle sizer (TDMPS) (Birmili et al., 1999) and an aerodynamic particle sizer (APS, model 3321, TSI Inc.). The mass concentrations of sulfate, nitrate, ammonium, organic matter (OM) and chloride (aerodynamic diameter less than 1 µm) were measured by an aerosol mass spectrometer (AMS, Aerodyne Inc.). The equivalent mass concentration of black carbon (EBC) was measured by a multi angle absorption photometer (MAAP, model 5012, Thermo Scientific Inc.) at 670 nm wavelength, the assumed mass absorption cross-section was 6.6 $m^2 g^{-1}$. Visibility was measured using a near-forward scattering sensor (FD12, Vaisala). Meteorological data were provided by the LinAn Regional Atmosphere Background Station.

All the instruments were housed in a measurement laboratory where room temperature was controlled at ~ 25 °C. All data were reported in Beijing Time (BJT = UTC + 8 h) and all the scattering data were referenced at T = 0 °C and P = 1013.25 hPa. Truncation error correction, proposed by Anderson and Ogren (1998), was applied to retrieve the final scattering and backscattering coefficients. The hemispheric backscatter fraction (b) was derived from equation $b = \sigma_{bsp}/\sigma_{sp}$ as mentioned above. The Ångström exponent was defined as å = $-\log[\sigma_{sp}(\lambda_1)/\sigma_{sp}(\lambda_2)]/\log[\lambda_1/\lambda_2]$. It represented the wavelength dependence of light scattering assuming a power law relationship of σ_{sp} and σ_{bsp}. In this study, scattering coefficients at 450 and 700 nm were used to derive . Normalization of f(RH) (Day and Malm, 2001) has been carried out to get the final f(RH) scan values, i.e. f(40 %) (the lowest RH in one cycle) is set to 1 and used to normalize other f(RH) values in this cycle. It's worth mentioning that the normalization of f(RH)

ACPD
15, 2853–2904, 2015

(see Sect. 2.2) may underestimate f(RH) to some extent, since some organics (e.g. humic acid sodium) take up water even when RH < 40 % (Sjogren et al., 2007; Dick et al., 2000). To evaluate its impact, we calculated the unnormalized f(40 %) with the raw data. The average and standard deviation were 1.03 and 0.03 with a maximum of 1.08, which means this normalization may cause an underestimate of 5 % (an error of 3 % was caused by the inconsistent of DryNeph and WetNeph, see Fig. 2) at most.

2.3 Inlet system

An automatic regenerating adsorption aerosol dryer (Tuch et al., 2009) was used to provide low RH sample air to DryNeph, TDMPS, APS, AMS and MAAP to ensure comparability of measurements. The aerosol dryer was housed in a separate shelter which was located on the rooftop (~ 5 m a.g.l.) of the measurement laboratory. Aerosols entered the shelter through a commercially available PM_{10} impactor (PM_{10} inlet, URG Corporation). Then these particles went through the adsorption aerosol dryer (Tuch et al., 2009) to ensure the RH less than 30 %. The dried aerosols passed through a splitter via 3/4″ stainless steel tubes, and then reached different instruments. The total sample flow through this dryer inlet was kept at 16.7 lpm to ensure a 50 % collection efficiency at 10 µm aerodynamic diameter (Berner et al., 1979). Since a lot of instruments share the total flow, the sample flow for the Nephelometer is 9 lpm.

2.4 Quality control on scattering measurements

Accurate performance of nephelometers and RH sensors is crucial to retrieve reliable enhancement factors (f(RH, λ), f_b(RH, λ) and f_β(RH, λ)), since they are defined as the ratio of aerosol scattering coefficient/backscattering coefficient/hemispheric backscatter fraction at a higher RH to those at a low RH (< 30 %). In addition, the RH control in the WetNeph sensing volume is also critical to f(RH) measurement. Therefore, several comparisons and calibrations have been carried out before and during the experiment. Three external RH sensors (Vaisala, model HMP60) were calibrated in the RH range of

ACPD
15, 2853–2904, 2015

11 to 80 % using Vaisala Humidity Calibrator (HMK15) with four saturated salt solutions (LiCl, K_2CO_3, NaCl, $(NH_4)_2SO_4$), and humidity/temperature transmitter (Vaisala, model HMT333), which was calibrated by the National Center for Meteorological Metrology, China. Two internal Nephelometer RH sensors were calibrated to the external RH sensors. Good agreement of these RH sensors were achieved with discrepancy < 3 %. Both nephelometers were calibrated with CO_2 (purity 99.999 %) and filtered air. Filtered air measurements were made automatically every hour to track the instrument stability. Comparison of scattering and backscattering coefficients of the two nephelometers under low RH (< 30 %) was performed during 1 to 3 March 2013 (as shown in Fig. 2). Total scattering coefficient and backscattering coefficient measured by WetNeph were, on average, ~ 3–4 % higher than those obtained by DryNeph at 550 nm (similarly for other wavelengths), which demonstrates that the two nephelometers were operating within their normal accuracy range.

The RH at the outlet of WetNeph was regulated via a feedback system between the Vaisala RH signal, a PID controller and a heater. The humidifier set point was stepped from low to high RH and back to low RH every hour with the set point changing every one or two minutes. Figure 3 is an example of our data showing the relative humidity control and corresponding scattering measurements. As can be seen from Fig. 3, good relative humidity control was achieved whether the scattering/backscattering coefficient was high or low.

The nephelometers were operated at a constant flow of 20 lpm, comprised of 9 lpm sample air and 11 lpm particle-free air (dilution flow). The total flowrate through the nephelometer was controlled by a mass flow controller. The dilution flow was regulated by a needle valve and measured by a mass flowmeter. The sample and dilution flow have been calibrated with a Gilibrator bubble flowmeter before the experiment. Filtered air tests have also been conducted to make sure that all the instruments were in good condition and that there were no leaks in the system.

ACPD
15, 2853–2904, 2015

3 Results and discussion

3.1 Overview

Figure 4 shows the time series of the measured and derived aerosol variables in March 2013, as well as the ambient RH and visibility. The scattering enhancement factor $f(85\,\%)$ ranged from 1.29 to 1.86 (as shown in Fig. 4a) with an average of 1.58 (Table 1) for the whole campaign. During 4–9 March, $f(85\,\%)$ stayed at a low value of 1.42 (±0.05) when LinAn was dominated by air masses from the south under clear sky. In March, the hourly averaged aerosol scattering coefficient (shown in Fig. 4c) varied from 21 to 1067 Mm^{-1} and the maximum occurred on 16 March, when a severe haze occurred. The mean value and standard deviation of the hourly averaged aerosol scattering coefficient was 223 Mm^{-1} (140 Mm^{-1}). Visibility (Fig. 4b) varied from 0.1 to 23.7 km with a mean value of 6.2 km. It was quite low on 23 and 24 March because the station was in cloud. From 15 to 16 March, visibility declined to 4.4 km with the accumulation of pollutants in the atmosphere, which was a severe haze episode (as mentioned above). An air mass from Northwest China with high dust levels arrived at LinAn on 10 March, with an abrupt increase of the aerosol scattering coefficient (Fig. 4c) and a sharp decline of Ångström exponent (Fig. 4d).

Based on nephelometer measurements, the enhancement factors for scattering coefficient $f(\mathrm{RH})$, backscattering coefficient $f_\mathrm{b}(\mathrm{RH})$ and hemispheric backscatter fraction $f_\beta(\mathrm{RH})$ were determined by Eqs. (1)–(3), respectively. As can be seen from Table 1, their values at different RHs (50, 60, 70, 80, and 85 %) were obtained using linear interpolation from the half-hourly humidogram data. The enhancement factors $f(\mathrm{RH})$ and $f_\mathrm{b}(\mathrm{RH})$ increased as the RH increased, but $f_\mathrm{b}(\mathrm{RH})$ increased much more slowly than $f(\mathrm{RH})$. The $f(85\,\%)$ and $f_\mathrm{b}(85\,\%)$ were 1.58 and 1.25, respectively, suggesting that the scattering coefficient and backscattering coefficient at 85 % RH were 58 and 25 % higher than those in dry conditions due to aerosol water uptake. The $f_\beta(\mathrm{RH})$ decreased with increasing RH, i.e. hemispheric backscatter fraction becomes smaller with the increase of RH and the fraction of radiation that would be backscattered into space was

ACPD
15, 2853–2904, 2015

reduced. The f_β(RH) decreased ~ 21 % as the RH increased from 40 to 85 %. All these parameters are of crucial importance in evaluating the aerosol radiative forcing.

Generally, the scattering enhancement factor (f(80 %) = 1.44) is much lower than the result (f(80 %) = 1.7–2.1) obtained by Xu et al. (2002) for LinAn in 1999. This value is also lower than the results obtained by Carrico during ACE-1 (Carrico et al., 1998) and ACE-Asia (Carrico et al., 2003), the values obtained by Zieger et al. (2013) in several European sites and the Arctic, as well as the values achieved by Malm and Day (Malm et al., 2003, 2005; Malm and Day, 2000, 2001; Day and Malm, 2001) in America. However, the difference between measured f(RH) in this study and previous studies performed in China (Yan et al., 2009; Pan et al., 2009; Liu et al., 2009; Delene and Ogren, 2002; Cheng et al., 2008) are much smaller. The enhancement factor for backscattering coefficient and hemispheric backscatter fraction (f_b(85 %) and f_β(85 %)) is 1.25(0.07) and 0.79(0.04), respectively, similar to the results (f_b(82 %) = 1.22 ± 0.06 and f_β(82 %) = 0.83) obtained by Carrico at Sagres, Portugal during ACE-2 (Carrico et al., 2000) and the results (f_b(82 %) = 1.27 and f_β(82 %) = 0.75) obtained by Carrico et al. (2003) during the dust-dominant period in ACE-Asia.

3.2 Aerosol chemical properties

The submicron mass concentration of sulfate, nitrate, ammonium, chloride and organic matter (OM) measured by AMS and EBC in PM_{10} measured by MAAP are summarized in Table 2. The mass concentration of OM is the largest, while the mass concentration of chloride is the smallest, in accord with previous studies in LinAn (Meng et al., 2012; Yan et al., 2005). The mean mass concentration of nitrate and sulfate were 9.8 ± 12.1 and 8.1 ± 4.1 μg m^{-3} in this study, similar to the values (9.4 ± 7.1 μg m^{-3} for nitrate and 8.6 ± 3.7 μg m^{-3} for sulfate in $PM_{2.5}$) at LinAn in 2010 summer (Meng et al., 2012).

Aerosol acidity is a key parameter affecting aerosol hygroscopic growth. It is usually examined by comparing the NH_4^+ mass concentration measured by AMS and the amount needed to fully neutralize sulfate, nitrate and chloride ions ($NH^+_{4\,\text{predicted}}$) (Sun

ACPD
15, 2853–2904, 2015

et al., 2010):

$$NH_{4\,\text{predicted}}^{+} = 18 \times \left(2 \cdot SO_4^{2-}/96 + NO_3^{-}/62 + Cl^{-}/35.5\right) \quad (4)$$

Figure 5 illustrates the relationship of measured NH_4^+ and predicted NH_4^+. As shown in Fig. 5, the regression slope is close to 1, which implies that there was sufficient NH_3 in the atmosphere to neutralize H_2SO_4, HNO_3 and HCl, and that the PM_1 aerosol at LinAn was bulk neutralized during the measurement period. Therefore, the dominant chemical form of sulfate aerosol is ammonium sulfate (AS) rather than acidic sulfate (H_2SO_4 or NH_4HSO_4) and the nitrate existed in the form of NH_4NO_3 (AN). By calculating Pearson's correlation coefficient among 5 different chemical compositions, it could be found that NH_4^+ and NO_3^- are strongly correlated with r = 0.93; NH_4^+ and SO_4^{2-}, Cl^- are highly related with r equal to 0.77 and 0.74 respectively, which also implies the main form of inorganics would be NH_4NO_3, $(NH_4)_2SO_4$ and NH_4Cl. However, because the average mass concentration of chloride was very low (see Table 2) at LinAn, it suggests that NH_4NO_3 and $(NH_4)_2SO_4$ are the dominant water-soluble ionic species, which are consistent with previous results at LinAn based on filter chemical measurements (Meng et al., 2012).

3.3 Wavelength dependence of the scattering enhancement factor *f*(85 %)

The wavelength dependence of scattering enhancement factor is needed to estimate the aerosol radiative forcing since solar radiation at Earth's surface depends on wavelength. The histograms for $f(85\,\%, 550\,\text{nm})$, $f(85\,\%, 550\,\text{nm}) - f(85\,\%, 450\,\text{nm})$ and $f(85\,\%, 550\,\text{nm}) - f(85\,\%, 700\,\text{nm})$ are shown in Fig. 6. Overlaid on the histogram for $f(85\,\%, 550\,\text{nm})$ (Fig. 6a) are Gaussian curves based on the statistics for $f(85\,\%)$ at each wavelength. No apparent shift of mean $f(85\,\%)$ is seen for the 550 and 700 nm wavelength pair (see Fig. 6a and c); while the mean $f(85\,\%, 450\,\text{nm})$ is ~ 6 % lower than that at 550 nm with a smaller standard deviation (see Fig. 6a and b). For higher values (90th and 70th percentile values in Table 3), slightly wavelength dependence of $f(\text{RH})$

ACPD
15, 2853–2904, 2015

can be observed, i.e. the f(RH) increases with the increase of wavelength. However, the differences are mostly under 10 % (see Fig. 6b and c) and therefore the discussion is focused on 550 nm wavelength in this study. Similar results were obtained by Zieger at a regional continental research site at Melpitz, Germany (Zieger et al., 2014).

3.4 Classification of various observation episodes

Based on wind direction, back trajectory analysis and weather phenomenon, observation periods can be classified into three main sectors: a northerly-polluted period (influenced by long-distance transport from northern China), a locally-polluted period, and a dust-influenced episode. Air mass back trajectories over 72 h at 300 m a.g.l. arrival height were calculated using the Trajectory Statistics (TrajStat) model (Wang et al., 2009) with 6 hourly archived meteorological data provided by the US National Centers for Environmental Prediction (NCEP). The characteristics of these three periods are as follows:

1. Periods when the wind direction is between 120 and 270° are chosen as "locally-polluted periods". During this period, pollutants mostly came from Anhui province, Jiangxi province and the southern region of Zhejiang province as well as LinAn (green line in Fig. 7). Economy in these areas is mainly made up of manufacturing, tourism and agriculture.

2. Periods when the wind direction is greater than 270° or less than 120° are described as "northerly-polluted periods". Back trajectories indicate that most of the air masses came from northern China and passed over heavily polluted areas such as the Beijing-Tianjin-Tangshan economic region and the Yangtze River Delta during long-distance transport (red line in Fig. 7).

3. A heavy dust event occurred at LinAn on 10 March (approximately from 02:00 BJT) according to satellite information (https://earthdata.nasa.gov/labs/worldview/) and 3 h meteorology information (provided by China Meteorological

ACPD
15, 2853–2904, 2015

Administration, CMA). The 72 h back trajectory shows the air masses tracked from Mongolia and passed over Inner Mongolia (blue line in Fig. 7).

3.4.1 Locally-polluted period

In the periods of 4–9, 15–20 and 26–30 March 2013 aerosols were mainly from locally mixed pollutants from Zhejiang and/or nearby provinces. The mean f(80 %) and f(85 %) were 1.36 and 1.52 (as shown in Table 4), ~ 10 and 8 % lower than those in northerly-polluted periods.

The enhancement factor for scattering coefficient and backscattering coefficients at 80 % during locally-polluted period is 1.36 and 1.15, respectively, similar to the values (f(82.5 %) = 1.4–1.5) and (f_β(82.5 %) = 1.1–1.2) obtained by Koloutsou-Vakakis et al. (2001) at a Northern Hemisphere, continental site (Bondville, Illinois, US). The measured dry scattering coefficient is 217 Mm^{-1}, ~ 15 % lower than that of the northerly-polluted period (251 Mm^{-1}). The averaged mass percentage of sulfate, nitrate, ammonium, OM, chloride and EBC are 17.6, 16.1, 13.0, 42.2, 1.5, and 9.6 %, respectively (shown in Fig. 7a). Compared to the northerly-polluted period, the mass percentage of OM is ~ 27 % higher during the locally-polluted period, while the mass percentage of nitrate is ~ 33 % lower. Although the $OM/(OM + SO_4^{2-})$ ratios during locally-polluted period (~ 0.70) and northerly-polluted period (~ 0.67) are similar, the $OM/(OM + NO_3^- + SO_4^{2-})$ ratio during locally-polluted period (~ 0.56) is 24 % higher than that during northerly-polluted period (~ 0.45), which may partly explain the lower f(RH) during locally-polluted episode (as discussed later in Sect. 3.5).

3.4.2 Northerly-polluted period

The air masses reaching LinAn during the period 1–3, 11–15, 20–26, and 30–31 March (dust episode excluded) mainly came from northern China through long-distance transport. The mean f(80 %) and f(85 %) were 1.50 and 1.64, respectively (as shown in Table 4).

ACPD
15, 2853–2904, 2015

The value (f(80 %) = 1.50) is similar to the previous results (f(80 %) = 1.48) obtained by Yan et al. (2009) for periods under the downwind of urban plume from Beijing, (f(80 %) = 1.46 ± 0.10) reported by Carrico et al. (2000) for anthropogenic aerosols in Europe during the 2nd Aerosol Characterization Experiment (ACE-2) campaign, and (f(80 %) = 1.55–1.59) indicated by Pan et al. (2009) for a rural site (Xin'an) near Beijing city during pollution periods. However, the measured f(80 %) was much lower than (f(80 %) = 2.0–2.43) during a pollution episode reported by Kim et al. (2006) at the Gosan regional background site, 720 km northeast of LinAn and results (f(82 %) = 2.24 ± 0.20) obtained by Carrico et al. (2003) in ACE-Asia for polluted air masses measured over the ocean. The f(RH) of continental air masses transported over the ocean was higher than that over the continent, and the possible mechanisms for that increase might include coagulation with sea-salt particles and the oxidation of SO_2 and VOCs (volatile organic compounds) to produce hygroscopic compounds.

3.4.3 Dust-influenced episode

During a severe cold air outbreak, northern China experienced a strong dust event on 8 and 9 March 2013. The affected area covered about 2.8 million square kilometers, of which the dust storm or strong sandstorm area covered about 0.27 million square kilometers, and is considered the widest and strongest dust event in 2013. During this process, suspended dust appeared in most of northwestern China, northern China, north and west Huanghuai region and west Liaoning province, the west-central Inner Mongolia, west Gansu, northern Shanxi, and several parts of Xinjiang experienced a sandstorm. Along with the extreme dust event, there was a dramatic increase in PM_{10}, for example, the PM_{10} in Yulin, Shanxi even reached 10 000 μg m^{-3} (Wang et al., 2013; Zhang and Sun, 2013).

At 2 a.m. on 10 March, wind direction changed abruptly to northerly (see Fig. 8d). The scattering coefficient increased abruptly from ~ 200 to > 600 Mm^{-1} (see Fig. 8b). PM_{10} mass concentrations at LinAn increased rapidly from 100 to 637 μg m^{-3}, while the $PM_{2.5}$ mass concentration was only 190 μg m^{-3}, accounting for 30 % of PM_{10}. The

ACPD
15, 2853–2904, 2015

Ångström exponent decreased from 1.2 to 0.8 (see Fig. 8c). All these phenomena implied the arrival of cold front from northern China enriched in coarse mode particles. The mass percentage of nitrate increased significantly and reached its peak (∼ 26 %) at 3 a.m.; meanwhile, the mass percentage of OM decreased sharply from 2 to 3 a.m. (see Fig. 8e). Correspondingly, the scattering enhancement factor $f(85\,\%)$ reached 1.52 at 3 a.m. (see Fig. 8a), an increase of ∼ 16 % compared with that before dust arrival. The most dust-dominated period, from 7 a.m. to 1 p.m., when Ångström exponent was below 0.5 (Fig. 8c) and scattering coefficients at 450, 550 and 700 nm (Fig. 8b) were almost the same, the scattering enhancement factor $f(85\,\%)$ was ∼ 1.46. This value is much higher than the results ($f(80\,\%) = 1.20$) reported by Pan et al. (2009) in rural Beijing, ($f(82.5\,\%) = 1.18$) obtained by Carrico et al. (2003) in East Asia (ACE-Asia) during a dust episode, ($f(80\,\%) = 1.20$) reported by Fierz-Schmidhauser et al. (2010) at a high alpine site (Jungfraujoch, 3580 m a.s.l.) in Switzerland during a strong Saharan dust event, and ($f(80\,\%) = 1.0$–1.1) measured by Li-Jones et al. (1998) in South America during an investigation of long-range transported Saharan dust. Meanwhile it is much lower than the value ($f(85\,\%) = 1.73$–2.20) obtained by Kim et al. (2006) in Gosan (South Korea) during a dust-dominated period. According to Tobo et al. (2010), Ca-rich particles can react with gaseous HNO_3 to form $Ca(NO_3)_2$, thus the liquid cloud-nucleating ability would be enhanced. Similar results have also reported that aerosol hygroscopicity would be largely enhanced if coarse mode Ca-rich particles combined with nitrate (Shi et al., 2008; Sullivan et al., 2009). Thus, it is speculated that the relatively high $f(RH)$ may have resulted from the reactions of coarse mode particles with inorganics (very likely to be nitrate) during long-range transport.

3.5 The relationship of scattering enhancement factor with chemical compositions

Scattering enhancement factor $f(85\,\%)$ vs. organic mass fraction and inorganic mass fraction were shown in Fig. 9. The total mass concentration was calculated as the sum

ACPD
15, 2853–2904, 2015

of mass concentrations of sulfate, nitrate, ammonium, chloride and organic measured by AMS and EBC measured by MAAP. The organic and inorganic mass fractions were calculated by dividing the mass concentration of organics (measured by AMS) and inorganics (the sum of sulfate, nitrate, ammonium and chloride measured by AMS) by the total mass concentration, respectively. As shown in Fig. 9, organics were clearly anti-correlated to $f(85\%)$, while inorganics showed strongly positive correlation with $f(85\%)$ ($R^2 = 0.86$). This implies that chemical composition plays a vital role in aerosol hygroscopic properties. The absolute values of both slopes (1.1 for $f(85\%)$ vs. organic mass fraction and 0.9 for $f(85\%)$ vs. inorganic mass fraction) were much lower than those (3.1 and 2.2, respectively) measured at Melpitz, Germany (Zieger et al., 2014). This may partly account to the higher organic (or lower inorganic) contents at LinAn. Comparing Fig. 9a and b with Fig. 9c and d, a more clearly trend of increasing nitrate with increasing $f(85\%)$ was observed. The role nitrate plays in aerosol hygroscopic properties will be discussed in the following paragraph.

$f(\mathrm{RH})$ in Fig. 10 was expressed in terms of γ so as to be applied to a broader RH range (Doherty et al., 2005; Quinn et al., 2005): $\gamma = \ln f(\mathrm{RH})/\ln((100 - \mathrm{RH_{ref}})/(100 - \mathrm{RH}))$. Here γ was based on $\mathrm{RH_{ref}} = 40\%$ and $\mathrm{RH} = 85\%$. The relative amount of OM and inorganics can be expressed as $\mathrm{Fo} = \mathrm{Cc}/(\mathrm{Cc} + C_\mathrm{i})$, where Cc and C_i are the mass concentrations of OM and inorganics, respectively. Figure 10 shows γ vs. Fo where C_i was the mass concentrations of SO_4^{2-}, NO_3^- and $NO_3^- + SO_4^{2-}$ in Fig. 10a, b, and c, respectively. For all the three scatter plots, there is a trend of decreasing γ with increasing Fo. However, unlike the results of Quinn et al. (2005), Malm et al. (2005), Pan et al. (2009) and Yan et al. (2009), γ and $\mathrm{Fo}(\mathrm{OM}/(\mathrm{OM}+\mathrm{SO_4^{2-}}))$ (shown in Fig. 10a) were uncorrelated ($R^2 = 0.14$), while γ and $\mathrm{Fo}(\mathrm{OM}/(\mathrm{OM} + \mathrm{NO_3^-}))$ (shown in Fig. 10b) and γ and $\mathrm{Fo}(\mathrm{OM}/(\mathrm{OM}+\mathrm{SO_4^{2-}}+\mathrm{NO_3^-}))$ (shown in Fig. 10c) were more strongly correlated (R^2 of 0.56 and 0.68, respectively). This result implies that NO_3^- (rather than SO_4^{2-}) plays an important role in aerosol hygroscopic growth during this study. This increasingly importance of nitrate corresponds to many recent studies in Shanghai (a mega city in Yangtze River Delta) (Shi et al., 2014) and Beijing (Sun et al., 2012). This may partly

ACPD
15, 2853–2904, 2015

result from increasing availability of NH_3 to form NH_4NO_3 (Morgan et al., 2010) due to the decrease of SO_2. Chinese government has put an emphasis on the control of SO_2 emission in recent years. The desulfurization technology were installed at coal-fired power units as well as certain steel and cement production facilities, as a result, the annual average concentration of SO_2 decreased significantly from 56 to 19 $\mu g\,m^{-3}$ at LinAn from 2006 to 2012 (ZEPB, 2006, 2012).

The molar ratio of particulate SO_4^{2-} to total sulfur (SO_4^{2-} + gas phase SO_2) was used as an indicator of the relative age of aerosols (Quinn et al., 2005). For relatively younger aerosols, there is insufficient time for the conversion of SO_2 to SO_4^{2-} via gas and aqueous phase oxidation process and therefore the $SO_4^{2-}/(SO_4^{2-}+SO_2)$ molar ratio is low. As aerosol ages, more SO_2 is converted to SO_4^{2-} and thus the ratio increases. To illustrate the effects of this ratio and scattering coefficient on γ, Fig. 11 shows γ vs. $Fo = OM/(OM+SO_4^{2-}+NO_3^-)$ colored by the $SO_4^{2-}/(SO_4^{2-}+SO_2)$ molar ratio (Fig. 11a) and $\log_{10}(\sigma_{sp})$ (Fig. 11b). The highest values of γ (or $f(RH)$) corresponded to more aged aerosols with a low OM content ; while the lowest values corresponded to younger aerosols with a higher OM content, consistent with the result of Quinn et al. (2005). For aerosols with relatively low scattering coefficient, the value of $f(RH)$ was usually low with a large variation (dots with cooler colors in Fig. 11b); while aerosols with high scattering coefficients, the value of $f(RH)$ was relatively high with a small variation (dots with warm colors in Fig. 11b).

3.6 Parameterization of scattering enhancement factor $f(RH)$

Scattering enhancement factor $f(RH)$ can be parameterized using empirical equations (Kotchenruther and Hobbs, 1998; Kotchenruther et al., 1999; Gassó et al., 2000; Carrico et al., 2003; Liu et al., 2008; Pan et al., 2009; Zieger et al., 2010, 2014). Humidograms of LinAn were fitted into two empirical equations and the fitting results were shown below.

ACPD
15, 2853–2904, 2015

3.6.1 Parameterization with equation $f(\mathrm{RH}) = c \cdot (1 - \mathrm{RH})^{-g}$

Kasten (1969) proposed an empirical equation $f(\mathrm{RH}) = c \cdot (1 - \mathrm{RH})^{-g}$ to describe how $f(\mathrm{RH})$ varies with RH, which has been used in previous reports e.g. by Kotchenruther and Hobbs (1998), Gassó et al. (2000), Carrico et al. (2003) and Zieger et al. (2010, 2014). Table 5 shows the fitting results of this work and other previous studies. The larger c and g, the larger $f(\mathrm{RH})$. In this work, g was much lower than that in most of the other studies, while was similar to the result of Gassó et al. (2000) during dust episode. It results from the comparably low scattering enhancement factor (e.g. $f(80\,\%) = 1.44 \pm 0.12$) of LinAn, which was similar to the value ($f(80\,\%) = 1.33 \pm 0.07$) obtained by Gassó et al. (2000) for a dust event. The $f(\mathrm{RH})$ in other studies was much higher than that at LinAn, ranging from 2.04 (polluted marine aerosols in Gassó et al. (2000)) to 3.77 (arctic aerosols in Zieger et al. (2010)), therefore their parameter g was much higher.

3.6.2 Parameterization with equation $f(\mathrm{RH}) = 1 + a \cdot \mathrm{RH}^b$

The $f(\mathrm{RH})$ obtained at LinAn station can be well described by the following equation, which was proposed by Kotchenruther and Hobbs (1998):

$$f(\mathrm{RH}) = 1 + a \cdot \mathrm{RH}^b \tag{5}$$

where a is positive and b is greater than 1. This function is convex, and has been used in many previous studies (Pan et al., 2009; Delene and Ogren, 2002; Carrico et al., 2003; Kotchenruther et al., 1999; Kotchenruther and Hobbs, 1998) to describe monotonic growth. Theoretically, parameter a determines the largest value $f(100\,\%)$ can reach, and parameter b dominates the curvature of the function. The smaller b is, the smaller the curvature of humidogram will be; if b equals to 1, then $f(\mathrm{RH}) = 1 + a \cdot \mathrm{RH}$. The parameters a and b from our study and previous results for different aerosol types are listed in Table 6. Taking the locally-polluted episode as an example, although parameter a is slightly larger ($\sim 3\,\%$) than in northerly-polluted episode, parameter b is $\sim 40\,\%$ greater, as a result the $f(85\,\%)$ during locally-polluted period is smaller. Parameter b is

ACPD
15, 2853–2904, 2015

the largest in the locally-polluted episode, and smallest in the northerly-polluted period, i.e. the curvature of RH – f(RH) line is largest during the locally-polluted episode, then is the dust episode, and northerly-polluted period is the smallest, which is consistent with the mass percentages of nitrate (see Fig. 7) (will be discussed later).

Among all the humidograms measured at LinAn, f(RH) increases continuously and monotonically. However, the curvatures of the humidograms are different (Fig. 12): some increase with a nearly constant rate and the humidogram line is almost straight, while some increase slowly at first and then increase more steeply at relatively higher RH, thus the curvature of the humidogram is greater. In order to describe the growth pattern quantitatively, a steepness index η is defined based on the fitting curve:

$$\eta = f'(80\,\%)/f'(60\,\%) - 1 = (4/3)^{b-1} - 1 \quad (6)$$

where $f'(60\,\%)$ and $f'(80\,\%)$ represent the derivatives of the fitting curve at 60 % and 80 % RH, respectively. η is a nonnegative number. Zieger et al. (2010) has defined an index describing the magnitude of deliquescence transitions based on fitting equation $f(\mathrm{RH}) = (1-\mathrm{RH})^{-g}$ (see Sect. 3.6.1), while the steepness index η proposed in this study provided a way of quantitatively describing the steepness of humidograms well fitted into equation $f(\mathrm{RH}) = 1 + a \cdot \mathrm{RH}^b$. The bigger η is, the greater the curvature. As is shown in Fig. 12a, for a large η, the $f'(60\,\%)$ is very small, meaning that aerosol scattering coefficient barely increases ($f(\mathrm{RH}) \approx 1$) under low RH (usually < 70 %). Once reaching larger RH ($\sim$ 70 %), f(RH) begins to increase. However, for a small η (Fig. 12b), the difference of the derivatives at 60 and 80 % RH was small, meaning the curvature of humidogram is much smaller.

A scatter plot of η and the mass percentage of nitrate is shown in Fig. 13, colored by the mass percentage of sulfate. As can be seen, η is negatively correlated with the mass percentage of nitrate. When the mass percentage of nitrate is below $\sim$ 18 %, the more nitrate, the smaller η is, which means the humidogram line becomes straighter and the difference of the derivatives at lower and higher RHs becomes smaller. For a mass percentage of nitrate higher than 18 % (correspondingly, a lower sulfate mass

ACPD
15, 2853–2904, 2015

percentage), η is ~ 1.1, meaning the humidogram line is almost straight (as shown in Fig. 12b) and aerosol scattering coefficient experiences a continuous and smooth growth at almost the same rate with RH.

3.7 Sensitivity of the direct radiative forcing of different aerosols to f(RH)

Direct radiative forcing of aerosols is quite sensitive to changes of relative humidity. The impact of relative humidity on globally-averaged, direct radiative forcing can be obtained by the following expression (Chylek and Wong, 1995):

$$\Delta F_{\mathrm{R}}(\mathrm{RH}) = -[S_0/4][T_{\mathrm{a}}^2(1-A_{\mathrm{c}})][2(1-R_{\mathrm{s}})^2\bar{\beta}(\mathrm{RH})M\alpha_{\mathrm{s}}f(\mathrm{RH}) - 4R_{\mathrm{s}}M\alpha_{\mathrm{a}}] \quad (7)$$

where S_0 is the solar constant, T_{a} is the transmittance of the atmosphere above the aerosol layer, A_{c} is the fractional cloud amount, R_{s} is the albedo of the underlying surface, $\bar{\beta}$(RH) is the solar radiation scattered back to space at defined RH, f(RH) is the scattering enhancement factor, M is the column burden of aerosol (in $\mathrm{g\,m^{-2}}$), α_{s} is the mass scattering efficiency, and α_{a} is the mass absorption efficiency.

In order to estimate the sensitivity of the forcing to the observed values of f(RH) for various aerosol types (locally-polluted, northerly-polluted and dust-influenced aerosols), the ratio of direct aerosol radiative forcing ΔF_{R} at a defined RH to that at dry condition was calculated:

$$\frac{\Delta F_{\mathrm{R}}(RH)}{\Delta F_{\mathrm{R}}(\mathrm{dry})} = \frac{(1-R_{\mathrm{s}})^2\bar{\beta}(\mathrm{RH})\alpha_{\mathrm{s}}f(\mathrm{RH}) - 2R_{\mathrm{s}}\alpha_{\alpha}}{(1-R_{\mathrm{s}})^2\bar{\beta}(\mathrm{dry})\alpha_{\mathrm{s}}f(\mathrm{dry}) - 2R_{\mathrm{s}}\alpha_{\alpha}} \quad (8)$$

Parameters used in Eq. (8) were $R_{\mathrm{s}} = 0.15$, and $\alpha_{\mathrm{a}} = 0.3\,\mathrm{m^2\,g^{-1}}$ (Wang et al., 2012; Hand and Malm, 2007). The mass scattering efficiency α_{s} is $2.76\,\mathrm{m^2\,g^{-1}}$, which is derived from the slope of a linear regression of the measured scattering coefficients and the calculated $\mathrm{PM_{10}}$ mass concentrations based on TDMPS and APS measurement (see Fig. 14); the high mass scattering efficiency is explained by the high ratio of $\mathrm{PM_1}$ to $\mathrm{PM_{10}}$ mass at this site (average 0.81). The average upscatter fraction $\bar{\beta}$

ACPD
15, 2853–2904, 2015

was calculated as $\bar{\beta} = 0.0817 + 1.8495b - 2.9682b^2$ (Delene and Ogren, 2002). The ratios $\Delta F_R(RH_{amb})/\Delta F_R(dry)$ for locally-polluted, northerly-polluted and dust-influenced aerosols are presented in Table 7, where $\Delta F_R(RH_{amb})$ was calculated at the ambient average realtive humidity (RH_{amb} = 67 %) in March at LinAn. The variables $f(RH_{amb})$, $b(RH_{amb})$, $\bar{\beta}(RH_{amb})$ and $\Delta F_R(RH_{amb})/\Delta F_R(dry)$ were the averages of the linear interpolation results of $f(RH)$, $b(RH)$, $\bar{\beta}(RH)$ and $\Delta F_R(RH)/\Delta F_R(dry)$ at 67 % RH.

As shown in Eq. (8), $f(RH)$ has a direct influence on the ratios $\Delta F_R(RH)/\Delta F_R(dry)$. At the ambient average RH of 67 %, the average $f(RH_{amb})$s for locally-polluted, northerly-polluted and dust-influenced aerosols were 1.17, 1.26 and 1.15, respectively, thus the ratios $\Delta F_R(RH_{amb})/\Delta F_R(dry)$ were 1.118, 1.195 and 1.105, respectively (see Table 7). That is to say the direct radiative forcing of locally-polluted, northerly-polluted and dust-influenced aerosols increased by 11.8, 19.5, and 10.5 % due to the aerosol hygroscopic growth at RH = 67 %. We could also see that the $f(RH)$ and the ratio $\Delta F_R(RH)/\Delta F_R(dry)$ for northerly-polluted aerosols were the largest, which suggests the effect of $f(RH)$ on direct radiative forcing is larger than that of the upscatter fraction $\bar{\beta}(RH)$, since $\bar{\beta}(RH)$ shows negative relationship with $f(RH)$.

4 Conclusions

The average enhancement factors and mean standard deviations at 85 % RH for scattering coefficient, backscattering coefficient and hemispheric backscatter fraction ($f(85\%)$, $f_b(85\%)$ and $f_\beta(85\%)$) were 1.58(0.12), 1.25(0.07) and 0.79(0.04), respectively, which means that at 85 % RH, the aerosol scattering coefficient and backscattering coefficient increased by 58 and 25 %. The mean values of $f(85\%)$ at 550 and 700 nm were similar; while the mean $f(85\%, 450\,nm)$ was approx. 6 % lower. Slight wavelength dependence of $f(85\%)$ was observed at higher $f(RH)$ values.

Our experimental data from LinAn station can be categorized into 3 episodes (northerly-polluted, locally-polluted and dust episodes) according to the wind direction, back trajectory and weather phenomenon. (1) During the locally-polluted period, air

ACPD
15, 2853–2904, 2015

masses mainly came from relatively clean districts, and the corresponding average and mean standard deviation of f(85 %), f_b(85 %) and f_β(85 %) were 1.52(0.10), 1.21(0.06) and 0.80(0.02), respectively; (2) During the northerly-polluted period, air masses came from northern China and passed through heavily polluted areas, and the average and mean standard deviation of f(85 %), f_b(85 %) and f_β(85 %) were 1.64(0.09), 1.28(0.06) and 0.78(0.02), respectively; (3) The average and mean standard deviation of f(85 %) during dust episode was 1.48(0.05), much higher than the values immediately before dust arrival.

Generally, the highest values of f(RH) corresponded to aged aerosols with a small fraction of OM; while the lowest values corresponded to younger aerosols with a larger fraction of OM. f(RH) of aerosols with relatively low scattering coefficient was usually low with a large variation; while f(RH) of aerosols with high scattering coefficients was relatively high with a small variation. Unlike the results of many previous reports like Quinn et al. (2005), Malm et al. (2005), Pan et al. (2009) and Yan et al. (2009), f(85 %) and $\mathrm{OM}/(\mathrm{OM}+\mathrm{SO_4^{2-}})$ were unrelated in this study, while $\mathrm{NO_3^-}$ plays an important role in determining the magnitude of f(RH) at LinAn.

The humidogram measured at LinAn can be well described by the model $f(\mathrm{RH}) = 1 + a \cdot \mathrm{RH}^b$, and the a and b for each episode are: 1.24 ± 0.29 and 5.46 ± 1.90 for locally-polluted period, 1.20 ± 0.21 and 3.90 ± 1.27 for northerly-polluted period, and 1.02 ± 0.19 and 4.51 ± 0.80 for dust episode. Further investigation shows the shape of the humidogram is closely related to the mass percentage of nitrate. A variable η has been defined to determine the degree of the curvature of humidogram. The more nitrate (or less sulfate), the smaller η is and the straighter the curve will be. When mass percentage of nitrate is larger than 18 %, most of η is approx. 1.1, which means the aerosol scattering increases continuously and monotonically with a nearly constant speed.

In March, the average relative humidity ($\mathrm{RH_{amb}}$) was 67 % and the averaged $f(\mathrm{RH_{amb}})$s for locally-polluted, northerly-polluted and dust-influenced aerosols were 1.17, 1.26 and 1.15, respectively. Correspondingly, the direct radiative forcing of locally-

ACPD
15, 2853–2904, 2015

polluted, northerly-polluted and dust-influenced aerosols increased by 11.8, 19.5, and 10.5 %, respectively due to aerosol uptake water in March at LinAn. In conclusion, water plays an important role in aerosol scattering properties as well as the radiative forcing, and it should be paid high attention when comparing between remote sensing and in-situ measurements and calculating the climate forcing.

Acknowledgements. This work was supported by National Basic Research Program of China (2011CB403401), the National Natural Science Foundation of China (41475118, 41175113), China International Science and Technology Cooperation Project (2009DFA22800), CAMS Basis Research Project (2010Z002, 2013Y004), and the Meteorological Special Project of China (GYHY-200906038, GYHY201206037). The authors would also like to thank the LinAn observational station staff for their support. The authors would thank D. Covert of U of W Atmospheric Sciences Seattle USA for useful discussions.

References

Ackerman, A. S., Kirkpatrick, M. P., Stevens, D. E., and Toon, O. B.: The impact of humidity above stratiform clouds on indirect aerosol climate forcing, Nature, 432, 1014–1017, 2004.

Adam, M., Putaud, J. P., Martins dos Santos, S., Dell'Acqua, A., and Gruening, C.: Aerosol hygroscopicity at a regional background site (Ispra) in Northern Italy, Atmos. Chem. Phys., 12, 5703–5717, doi:10.5194/acp-12-5703-2012, 2012.

Anderson, T., Covert, D., Marshall, S., Laucks, M., Charlson, R., Waggoner, A., Ogren, J., Caldow, R., Holm, R., and Quant, F.: Performance characteristics of a high-sensitivity, three-wavelength, total scatter/backscatter nephelometer, J. Atmos. Ocean. Tech., 13, 967–986, 1996.

Anderson, T. L. and Ogren, J. A.: Determining aerosol radiative properties using the TSI 3563 integrating nephelometer, Aerosol Sci. Tech., 29, 57–69, 1998.

Berner, A., Lürzer, C., Pohl, F., Preining, O., and Wagner, P.: The size distribution of the urban aerosol in Vienna, Sci. Total Environ., 13, 245–261, 1979.

Birmili, W., Stratmann, F., and Wiedensohler, A.: Design of a DMA-based size spectrometer for a large particle size range and stable operation, J. Aerosol Sci., 30, 549–553, 1999.

ACPD
15, 2853–2904, 2015

Carrico, C. M., Rood, M. J., and Ogren, J. A.: Aerosol light scattering properties at Cape Grim, Tasmania, during the first Aerosol Characterization Experiment (ACE 1), J. Geophys. Res., 103, 16565–16574, 1998.
Carrico, C. M., Rood, M. J., Ogren, J. A., Neusüß, C., Wiedensohler, A., and Heintzenberg, J.: Aerosol optical properties at Sagres, Portugal during ACE-2, Tellus B, 52, 694–715, 2000.
Carrico, C. M., Kus, P., Rood, M. J., Quinn, P. K., and Bates, T. S.: Mixtures of pollution, dust, sea salt, and volcanic aerosol during ACE-Asia: radiative properties as a function of relative humidity, J. Geophys. Res, 108, 8650, doi:10.1029/2003JD003405, 2003.
Charlson, R. J., Ahlquist, N., Selvidge, H., and MacCready Jr, P.: Monitoring of atmospheric aerosol parameters with the integrating nephelometer, JAPCA J. Air Waste Ma., 19, 937–942, 1969.
Charlson, R. J., Schwartz, S., Hales, J., Cess, R. D., Coakley, Jr., J. A., Hansen, J., and Hofmann, D.: Climate forcing by anthropogenic aerosols, Science, 255, 423–430, 1992.
Cheng, Y., Wiedensohler, A., Eichler, H., Heintzenberg, J., Tesche, M., Ansmann, A., Wendisch, M., Su, H., Althausen, D., and Herrmann, H.: Relative humidity dependence of aerosol optical properties and direct radiative forcing in the surface boundary layer at Xinken in Pearl River Delta of China: an observation based numerical study, Atmos. Environ., 42, 6373–6397, 2008.
Chylek, P. and Wong, J.: Effect of absorbing aerosols on global radiation budget, Geophys. Res. Lett., 22, 929–931, 1995.
Covert, D. S., Charlson, R., and Ahlquist, N.: A study of the relationship of chemical composition and humidity to light scattering by aerosols, J. Appl. Meteorol., 11, 968–976, 1972.
Day, D. E. and Malm, W. C.: Aerosol light scattering measurements as a function of relative humidity: a comparison between measurements made at three different sites, Atmos. Environ., 35, 5169–5176, 2001.
Delene, D. J. and Ogren, J. A.: Variability of aerosol optical properties at four North American surface monitoring sites, J. Atmos. Sci., 59, 1135–1150, 2002.
Dick, W. D., Saxena, P., and McMurry, P. H.: Estimation of water uptake by organic compounds in submicron aerosols measured during the Southeastern Aerosol and Visibility Study, J. Geophys. Res.-Atmos., 105, 1471–1479, 2000.
Doherty, S. J., Quinn, P. K., Jefferson, A., Carrico, C. M., Anderson, T. L., and Hegg, D.: A comparison and summary of aerosol optical properties as observed in situ from aircraft, ship, and land during ACE-Asia, J. Geophys. Res., 110, D04201, doi:10.1029/2004JD004964, 2005.

ACPD
15, 2853–2904, 2015

Engelhart, G. J., Hildebrandt, L., Kostenidou, E., Mihalopoulos, N., Donahue, N. M., and Pandis, S. N.: Water content of aged aerosol, Atmos. Chem. Phys., 11, 911–920, doi:10.5194/acp-11-911-2011, 2011.
Fang, S. X., Zhou, L. X., Masarie, K. A., Xu, L., and Rella, C. W.: Study of atmospheric CH4 mole fractions at three WMO/GAW stations in China, J. Geophys. Res.-Atmos., 118, 4874–4886, 2013.
Fierz-Schmidhauser, R., Zieger, P., Gysel, M., Kammermann, L., DeCarlo, P. F., Baltensperger, U., and Weingartner, E.: Measured and predicted aerosol light scattering enhancement factors at the high alpine site Jungfraujoch, Atmos. Chem. Phys., 10, 2319–2333, doi:10.5194/acp-10-2319-2010, 2010.
Hänel, G.: The properties of atmospheric aerosol particles as functions of the relative humidity at thermodynamic equilibrium with the surrounding moist air, Adv. Geophys., 19, 73–188, 1976.
Hand, J. and Malm, W.: Review of aerosol mass scattering efficiencies from ground-based measurements since 1990, J. Geophys. Res.-Atmos., 112, D16203, doi:10.1029/2007JD008484, 2007.
Kim, J., Yoon, S.-C., Jefferson, A., and Kim, S.-W.: Aerosol hygroscopic properties during Asian dust, pollution, and biomass burning episodes at Gosan, Korea in April 2001, Atmos. Environ., 40, 1550–1560, 2006.
Koloutsou-Vakakis, S., Carrico, C., Kus, P., Rood, M., Li, Z., Shrestha, R., Ogren, J., Chow, J., and Watson, J.: Aerosol properties at a midlatitude Northern Hemisphere continental site, J. Geophys. Res., 106, 3019–3032, 2001.
Kotchenruther, R. A. and Hobbs, P. V.: Humidification factors of aerosols from biomass burning in Brazil, J. Geophys. Res., 103, 32081–32089, doi:10.1029/98jd00340, 1998.
Kotchenruther, R. A., Hobbs, P. V., and Hegg, D. A.: Humidification factors for atmospheric aerosols off the mid-Atlantic coast of the United States, J. Geophys. Res., 104, 2239–2251, 1999.
Li-Jones, , X., Maring, H. B., and Prospero, J. M.: Effect of relative humidity on light scattering by mineral dust aerosol as measured in the marine boundary layer over the tropical Atlantic Ocean, J. Geophys. Res., 103, 31113–31121, 1998.
Liu, X., Zhang, Y., Jung, J., Gu, J., Li, Y., Guo, S., Chang, S.-Y., Yue, D., Lin, P., Kim, Y. J., Hu, M., Zeng, L., and Zhu, T.: Research on the hygroscopic properties of aerosols by mea-

ACPD
15, 2853–2904, 2015

surement and modeling during CAREBeijing-2006, J. Geophys. Res.-Atmos., 114, D00G16, doi:10.1029/2008JD010805, 2009.
Magi, B. I. and Hobbs, P. V.: Effects of humidity on aerosols in southern Africa during the biomass burning season, J. Geophys. Res.-Atmos., 108, 8504, doi:10.1029/2002JD002144, 2003.
Malm, W. C. and Day, D. E.: Optical properties of aerosols at Grand Canyon national park, Atmos. Environ., 34, 3373–3391, 2000.
Malm, W. C. and Day, D. E.: Estimates of aerosol species scattering characteristics as a function of relative humidity, Atmos. Environ., 35, 2845–2860, 2001.
Malm, W. C., Day, D. E., Kreidenweis, S. M., Collett, J. L., and Lee, T.: Humidity-dependent optical properties of fine particles during the big bend regional aerosol and visibility observational study, J. Geophys. Res., 108, 4279, doi:10.1029/2002JD002998, 2003.
Malm, W. C., Day, D. E., Kreidenweis, S. M., Collett, J. L., Carrico, C., McMeeking, G., and Lee, T.: Hygroscopic properties of an organic-laden aerosol, Atmos. Environ., 39, 4969–4982, 2005.
Meng, Z. Y., Jia, X. F., Zhang, R. J., Yu, X. M., and Ma, Q. L.: Characteristics of $PM_{2.5}$ at Lin'an regional background station in the Yangtze River Delta region, J. Appl. Meteorol. Sci., 23, 424–432, 2012.
Morgan, W. T., Allan, J. D., Bower, K. N., Esselborn, M., Harris, B., Henzing, J. S., Highwood, E. J., Kiendler-Scharr, A., McMeeking, G. R., Mensah, A. A., Northway, M. J., Osborne, S., Williams, P. I., Krejci, R., and Coe, H.: Enhancement of the aerosol direct radiative effect by semi-volatile aerosol components: airborne measurements in North-Western Europe, Atmos. Chem. Phys., 10, 8151–8171, doi:10.5194/acp-10-8151-2010, 2010.
Pan, L., Che, H., Geng, F., Xia, X., Wang, Y., Zhu, C., Chen, M., Gao, W., and Guo, J.: Aerosol optical properties based on ground measurements over the Chinese Yangtze Delta region, Atmos. Environ., 44, 2587–2596, 2010.
Pan, X. L., Yan, P., Tang, J., Ma, J. Z., Wang, Z. F., Gbaguidi, A., and Sun, Y. L.: Observational study of influence of aerosol hygroscopic growth on scattering coefficient over rural area near Beijing mega-city, Atmos. Chem. Phys., 9, 7519–7530, doi:10.5194/acp-9-7519-2009, 2009.
Pilinis, C., Seinfeld, J. H., and Grosjean, D.: Water content of atmospheric aerosols, Atmos. Environ., 23, 1601–1606, 1989.
Pilinis, C., Pandis, S. N., and Seinfeld, J. H.: Sensitivity of direct climate forcing by atmospheric aerosols to aerosol size and composition, J. Geophys. Res., 100, 18739–18754, 1995.

ACPD
15, 2853–2904, 2015

Qi, H., Lin, W., Xu, X., Yu, X., and Ma, Q.: Significant downward trend of SO2 observed from 2005 to 2010 at a background station in the Yangtze Delta region, China, Sci. China Ser. B, 55, 1451–1458, 2012.
Quinn, P., Marshall, S., Bates, T., Covert, D., and Kapustin, V.: Comparison of measured and calculated aerosol properties relevant to the direct radiative forcing of tropospheric sulfate aerosol on climate, J. Geophys. Res., 100, 8977–8991, 1995.
Quinn, P. K., Bates, T. S., Baynard, T., Clarke, A. D., Onasch, T. B., Wang, W., Rood, M. J., Andrews, E., Allan, J., Carrico, C. M., Coffman, D., and Worsnop, D.: Impact of particulate organic matter on the relative humidity dependence of light scattering: a simplified parameterization, Geophys. Res. Lett., 32, L22809, doi:10.1029/2005gl024322, 2005.
Randles, C., Russell, L., and Ramaswamy, V.: Hygroscopic and optical properties of organic sea salt aerosol and consequences for climate forcing, Geophys. Res. Lett., 31, L16108, doi:10.1029/2004GL020628, 2004.
Shen, X. J., Sun, J. Y., Zhang, Y. M., Wehner, B., Nowak, A., Tuch, T., Zhang, X. C., Wang, T. T., Zhou, H. G., Zhang, X. L., Dong, F., Birmili, W., and Wiedensohler, A.: First long-term study of particle number size distributions and new particle formation events of regional aerosol in the North China Plain, Atmos. Chem. Phys., 11, 1565–1580, doi:10.5194/acp-11-1565-2011, 2011.
Shi, Y., Chen, J., Hu, D., Wang, L., Yang, X., and Wang, X.: Airborne submicron particulate (PM_1) pollution in Shanghai, China: chemical variability, formation/dissociation of associated semi-volatile components and the impacts on visibility, Sci. Total Environ., 473, 199–206, 2014.
Shi, Z., Zhang, D., Hayashi, M., Ogata, H., Ji, H., and Fujiie, W.: Influences of sulfate and nitrate on the hygroscopic behaviour of coarse dust particles, Atmos. Environ., 42, 822–827, 2008.
Sjogren, S., Gysel, M., Weingartner, E., Baltensperger, U., Cubison, M., Coe, H., Zardini, A., Marcolli, C., Krieger, U., and Peter, T.: Hygroscopic growth and water uptake kinetics of two-phase aerosol particles consisting of ammonium sulfate, adipic and humic acid mixtures, J. Aerosol Sci., 38, 157–171, 2007.
Sullivan, R. C., Moore, M. J. K., Petters, M. D., Kreidenweis, S. M., Roberts, G. C., and Prather, K. A.: Effect of chemical mixing state on the hygroscopicity and cloud nucleation properties of calcium mineral dust particles, Atmos. Chem. Phys., 9, 3303–3316, doi:10.5194/acp-9-3303-2009, 2009.

ACPD
15, 2853–2904, 2015

Sun, J., Zhang, Q., Canagaratna, M. R., Zhang, Y., Ng, N. L., Sun, Y., Jayne, J. T., Zhang, X., Zhang, X., and Worsnop, D. R.: Highly time-and size-resolved characterization of submicron aerosol particles in Beijing using an aerodyne aerosol mass spectrometer, Atmos. Environ., 44, 131–140, 2010.

Sun, Y., Wang, Z., Dong, H., Yang, T., Li, J., Pan, X., Chen, P., and Jayne, J. T.: Characterization of summer organic and inorganic aerosols in Beijing, China with an aerosol chemical speciation monitor, Atmos. Environ., 51, 250–259, 2012.

Tang, I. N.: Chemical and size effects of hygroscopic aerosols on light scattering coefficients, J. Geophys. Res.-Atmos., 101, 19245–19250, 1996.

Tobo, Y., Zhang, D., Matsuki, A., and Iwasaka, Y.: Asian dust particles converted into aqueous droplets under remote marine atmospheric conditions, P. Natl. Acad. Sci. USA, 107, 17905–17910, 2010.

Tuch, T. M., Haudek, A., Müller, T., Nowak, A., Wex, H., and Wiedensohler, A.: Design and performance of an automatic regenerating adsorption aerosol dryer for continuous operation at monitoring sites, Atmos. Meas. Tech., 2, 417–422, doi:10.5194/amt-2-417-2009, 2009.

Wang, Y., Zhang, X., and Draxler, R. R.: TrajStat: GIS-based software that uses various trajectory statistical analysis methods to identify potential sources from long-term air pollution measurement data, Environ. Modell. Softw., 24, 938–939, 2009.

Wang, J. and Martin, S. T.: Satellite characterization of urban aerosols: Importance of including hygroscopicity and mixing state in the retrieval algorithms, J. Geophys. Res.-Atmos., 112, D17203, doi:10.1029/2006JD008078, 2007.

Wang, M. X., Ding, X., Fu, X., He, Q., Wang, S., Bernard, F., Zhao, X., and Wu, D.: Aerosol scattering coefficients and major chemical compositions of fine particles observed at a rural site in the central Pearl River Delta, South China, J. Environ. Sci., 24, 72–77, 2012.

Wang, L. P., Zhang, B. H., and Zhang, X. W.: Main weather processes in March and April, 2013, Weather Forecast Rev., 5, 1–7, 2013.

Weingartner, E., Baltensperger, U., and Burtscher, H.: Growth and structural change of combustion aerosols at high relative humidity, Environ. Sci. Technol., 29, 2982–2986, 1995.

Wiscombe, W. and Grams, G.: The backscattered fraction in two-stream approximations, J. Atmos. Sci., 33, 2440–2451, 1976.

Xia, X., Li, Z., Holben, B., Wang, P., Eck, T., Chen, H., Cribb, M., and Zhao, Y.: Aerosol optical properties and radiative effects in the Yangtze Delta region of China, J. Geophys. Res.-Atmos., 112, D22S12, doi:10.1029/2007JD008859, 2007.

ACPD
15, 2853–2904, 2015

Xu, J., Bergin, M., Yu, X., Liu, G., Zhao, J., Carrico, C., and Baumann, K.: Measurement of aerosol chemical, physical and radiative properties in the Yangtze Delta region of China, Atmos. Environ., 36, 161–173, 2002.
Xu, X., Lin, W., Wang, T., Yan, P., Tang, J., Meng, Z., and Wang, Y.: Long-term trend of surface ozone at a regional background station in eastern China 1991–2006: enhanced variability, Atmos. Chem. Phys., 8, 2595–2607, doi:10.5194/acp-8-2595-2008, 2008.
Yan, P., Zhang, Y. M., Yang, D. Z., Tang, J., Yu, X. L., Cheng, H. B., and Yu, X. M.: The charactertistic of aerosol ionic size distributions at Lin'an in summer of 2003, Acta Meteor. Sin., 63, 980–987, 2005.
Yan, P., Pan, X., Tang, J., Zhou, X., Zhang, R., and Zeng, L.: Hygroscopic growth of aerosol scattering coefficient: A comparative analysis between urban and suburban sites at winter in Beijing, Particuology, 7, 52–60, 2009.
Zhang, B. and Sun, J.: Analysis of the March 2013 atmospheric circulation and Weather, Meteor. Mon., 39, 794–800, 2013.
Zhang, Y. Y., Zuo, L. F., Ren, X. C., and Cui, J.: Research of the aerosol scattering properties based on evaporation duct, Ship Electron. Eng., 32, 12–14, 2012.
Zhejiang Environmental Protection Bureau (ZEPB), 2006, Annual Report on the State of the Environment of Zhejiang Province, Zhejiang Environmental Protection Bureau, Hangzhou, 21 pp., 2006.
Zhejiang Environmental Protection Bureau (ZEPB), 2012, Annual Report on the State of the Environment of Zhejiang Province, Zhejiang Environmental Protection Bureau, Hangzhou, 29 pp., 2012.
Zieger, P., Fierz-Schmidhauser, R., Gysel, M., Ström, J., Henne, S., Yttri, K. E., Baltensperger, U., and Weingartner, E.: Effects of relative humidity on aerosol light scattering in the Arctic, Atmos. Chem. Phys., 10, 3875–3890, doi:10.5194/acp-10-3875-2010, 2010.
Zieger, P., Weingartner, E., Henzing, J., Moerman, M., de Leeuw, G., Mikkilä, J., Ehn, M., Petäjä, T., Clémer, K., van Roozendael, M., Yilmaz, S., Frieß, U., Irie, H., Wagner, T., Shaiganfar, R., Beirle, S., Apituley, A., Wilson, K., and Baltensperger, U.: Comparison of ambient aerosol extinction coefficients obtained from in-situ, MAX-DOAS and LIDAR measurements at Cabauw, Atmos. Chem. Phys., 11, 2603–2624, doi:10.5194/acp-11-2603-2011, 2011.
Zieger, P., Kienast-Sjögren, E., Starace, M., von Bismarck, J., Bukowiecki, N., Baltensperger, U., Wienhold, F. G., Peter, T., Ruhtz, T., Collaud Coen, M., Vuilleumier, L., Maier, O., Emili, E.,

ACPD
15, 2853–2904, 2015

Popp, C., and Weingartner, E.: Spatial variation of aerosol optical properties around the high-alpine site Jungfraujoch (3580 m a.s.l.), Atmos. Chem. Phys., 12, 7231–7249, doi:10.5194/acp-12-7231-2012, 2012.

Zieger, P., Fierz-Schmidhauser, R., Weingartner, E., and Baltensperger, U.: Effects of relative humidity on aerosol light scattering: results from different European sites, Atmos. Chem. Phys., 13, 10609–10631, doi:10.5194/acp-13-10609-2013, 2013.

Zieger, P., Fierz-Schmidhauser, R., Poulain, L., Müller, T., Birmili, W., Spindler, G., Wiedensohler, A., Baltensperger, U., and Weingartner, E.: Influence of water uptake on the aerosol-particle light scattering coefficients of the Central European aerosol, Tellus B, 66, 22716, doi:10.3402/tellusb.v66.22716, 2014.

ACPD
15, 2853–2904, 2015

Table 1. Averaged enhancement factors and mean standard deviations for scattering coefficient, backscattering coefficient and hemispheric backscatter fraction at different RHs.

RH(%)	f(RH)	f_b(RH)	f_β(RH)
50	1.07(0.04)	1.04(0.02)	0.96(0.02)
60	1.14(0.08)	1.06(0.04)	0.93(0.04)
70	1.24(0.11)	1.10(0.05)	0.89(0.05)
80	1.43(0.12)	1.18(0.07)	0.83(0.05)
85	1.58(0.12)	1.25(0.07)	0.79(0.04)

ACPD
15, 2853–2904, 2015

Table 2. Summary of mass concentrations ($\mu g\,m^{-3}$) of aerosol species measured by AMS as well as MAAP* (SD: standard deviation).

	Mean	SD	Minimum	Maximum
Sulfate	8.1	4.1	0.1	26.1
Nitrate	9.8	12.1	0.2	79.2
Ammonium	6.9	5.5	0.5	42.8
Chloride	1.1	2.0	0.002	22.9
OM	17.7	11.1	2.8	93.9
EBC*	4.1	2.8	0.7	25.3

* EBC was meausured by MAAP in PM_{10}.

ACPD
15, 2853–2904, 2015

Table 3. Statistical values of $f(85\%)$ at 450, 550, and 700 nm wavelengths (SD: standard deviation; prctl: percentile).

λ	mean	SD	90th prctl.	75th prctl.	median	25th prctl.	10th prctl.
450 nm	1.51	0.09	1.63	1.58	1.53	1.47	1.39
550 nm	1.58	0.12	1.72	1.65	1.59	1.49	1.40
700 nm	1.59	0.15	1.77	1.70	1.62	1.46	1.36

ACPD
15, 2853–2904, 2015

Table 4. Average enhancement factors and mean standard deviations for scattering coefficient, backscattering coefficient and hemispheric backscatter fraction in various observation episodes.

	Locally-polluted	Northerly-polluted	Dust-influenced
$f(80\,\%)$	1.36(0.11)	1.50(0.09)	1.37(0.05)
$f_b(80\,\%)$	1.15(0.06)	1.21(0.06)	1.15(0.03)
$f_\beta(80\,\%)$	0.85(0.04)	0.81(0.03)	0.84(0.03)
$f(85\,\%)$	1.52(0.10)	1.64(0.09)	1.48(0.05)
$f_b(85\,\%)$	1.21(0.06)	1.28(0.06)	1.19(0.04)
$f_\beta(85\,\%)$	0.80(0.02)	0.78(0.02)	0.81(0.03)
N	295	303	14

ACPD
15, 2853–2904, 2015

Table 5. Curve-fitting parameters for various aerosol types in terms of equation $f(\mathrm{RH}) = c \cdot (1 - \mathrm{RH})^{-g}$.

	c	g	Reference
Locally-polluted	0.85 ± 0.08	0.29 ± 0.04	
Northerly-polluted	0.93 ± 0.07	0.28 ± 0.03	This work
Dust-influenced	0.87 ± 0.05	0.27 ± 0.02	
Continental	0.9 ± 0.1	–	Zieger et al. (2014)
Arctic[a]	1	0.58 ± 0.09	Zieger et al. (2010)
Marine	0.99	0.54	
Polluted	0.59	0.77	Carrico et al. (2003)
Dust	0.60	0.61	
Polluted Marine	1	0.57 ± 0.06	Gassó et al. (2000)
Dust	1	0.23 ± 0.05	
Clean Marine1[b]	1	0.69 ± 0.06	
Clean Marine2[c]	1	0.73 ± 0.07	

[a] fitting results for aerosol samples with RH > 75 %.
[b] fitting results for aerosol samples with RH > 60 %.
[c] fitting results for aerosol samples with RH > 80 %.

ACPD
15, 2853–2904, 2015

Table 6. Curve-fitting parameters for various aerosol types in terms of Eq. (5) $f(\mathrm{RH}) = 1 + a \cdot \mathrm{RH}^b$.

	a	b	Reference
Locally-polluted	1.24 ± 0.29	5.46 ± 1.90	
Northerly-polluted	1.20 ± 0.21	3.90 ± 1.27	This work
Dust-influenced	1.02 ± 0.19	4.51 ± 0.80	
Clean	1.20 ± 0.06	6.07 ± 0.27	
Polluted	2.30 ± 0.03	6.27 ± 0.10	Pan et al. (2009)
Dust	0.64 ± 0.04	5.17 ± 0.40	
Urban	2.06	3.60	
Mixed	3.26	3.85	Liu et al. (2007)
Marine	4.92	5.04	

ACPD
15, 2853–2904, 2015

Table 7. Estimated effects of aerosol hygroscopic growth on direct radiative forcing by locally-polluted, northerly-polluted and dust-influenced aerosols at LinAn, measured by the ratio ($\Delta F_R(RH_{amb})/\Delta F_R(dry)$) of direct aerosol radiative forcing at the ambient average relative humidity (RH_{amb} = 67 %) for the entire campaign to that in dry condition.

	$f(RH_{amb})$	$b(dry)$	$\bar{\beta}(dry)$	$b(RH_{amb})$	$\bar{\beta}(RH_{amb})$	$\Delta F_R(RH_{amb})/\Delta F_R(dry)$
Entire campaign	1.21	0.126	0.268	0.115	0.255	1.157
Locally-polluted	1.17	0.131	0.274	0.123	0.263	1.118
Northerly-polluted	1.26	0.121	0.262	0.106	0.243	1.195
Dust-influenced	1.15	0.146	0.289	0.132	0.274	1.105

ACPD
15, 2853–2904, 2015

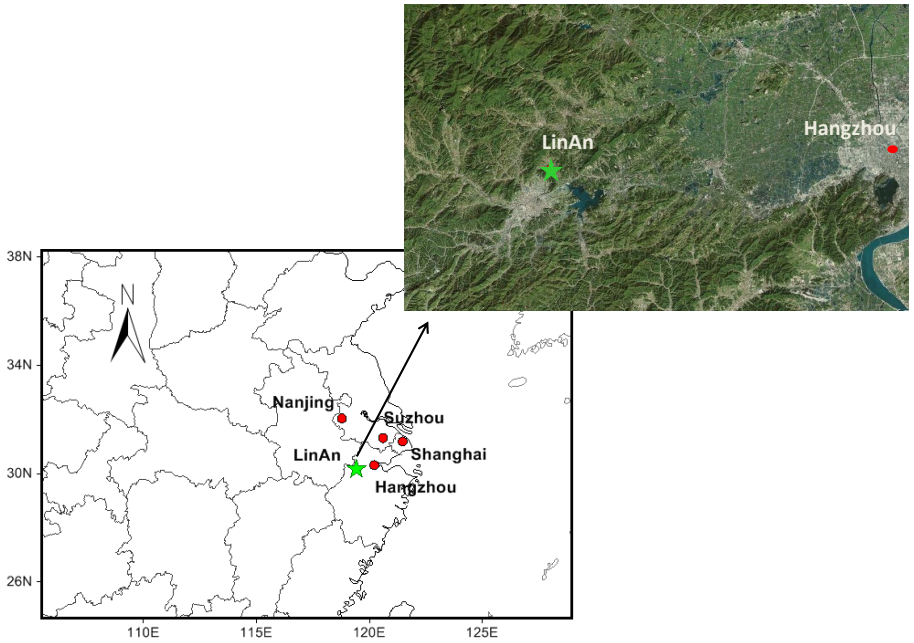

Figure 1. Location of LinAn station (green pentagram) and the main cities in the Yangtze River Delta (red dots) in the lower left panel. The upper right panel is the topography of the surrounding area.

ACPD
15, 2853–2904, 2015

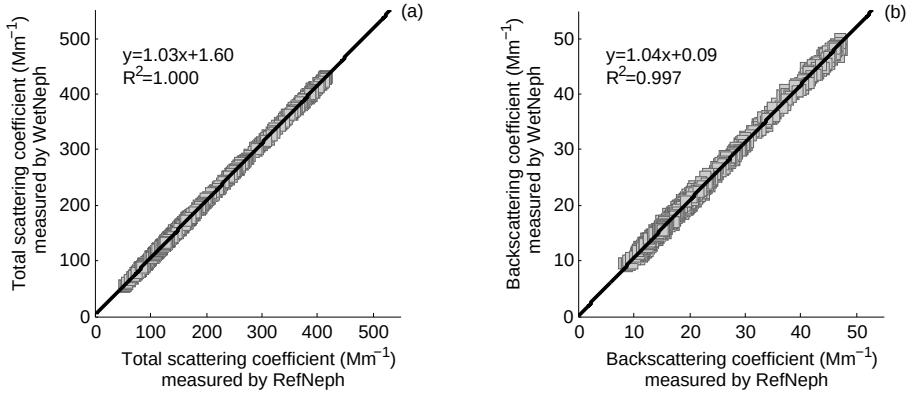

Figure 2. Comparison of **(a)** scattering coefficient and **(b)** backscattering coefficient measured by DryNeph and WetNeph, both under reference dry conditions (RH < 30 %) on 1–3 March 2013. The solid black lines represent linear least square regression.

ACPD
15, 2853–2904, 2015

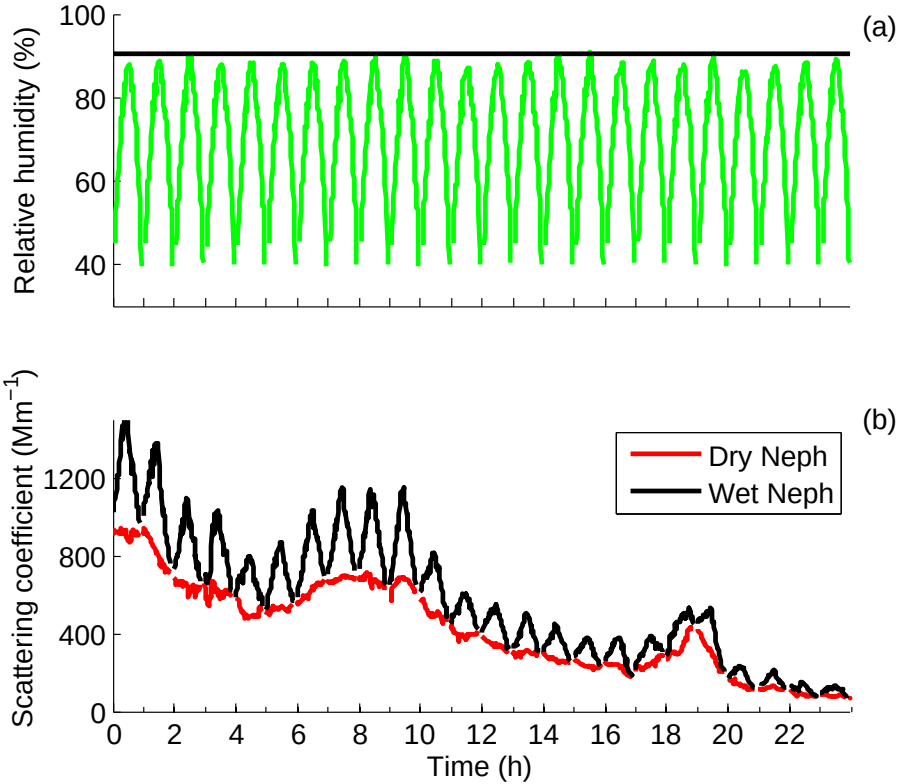

Figure 3. Example of recorded data on 17 March 2013 **(a)** Relative humidity of WetNeph, the black line represents RH = 91 %; **(b)** Aerosol scattering coefficients measured by DryNeph (red line) and WetNeph (black line).

ACPD
15, 2853–2904, 2015

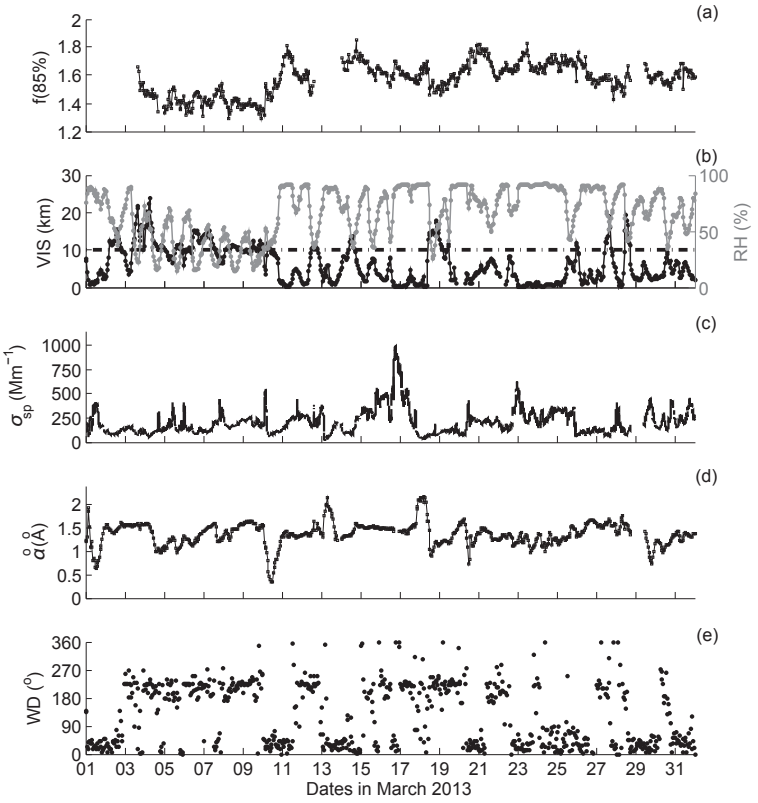

Figure 4. Time series of measured and derived aerosol variables, as well as the ambient RH and visibility. **(a)** scattering enhancement factor at RH = 85 %; **(b)** visibility (VIS) and relative humidity (RH) at ambient conditions, the dashed line represents VIS = 10 km; **(c)** aerosol scattering coefficient of DryNeph at 550 nm wavelength; **(d)** Ångström exponent ; **(e)** wind direction (WD), indicating prevailing wind directions during observation period was mainly northeasterly (NE) and southwesterly (SW).

ACPD
15, 2853–2904, 2015

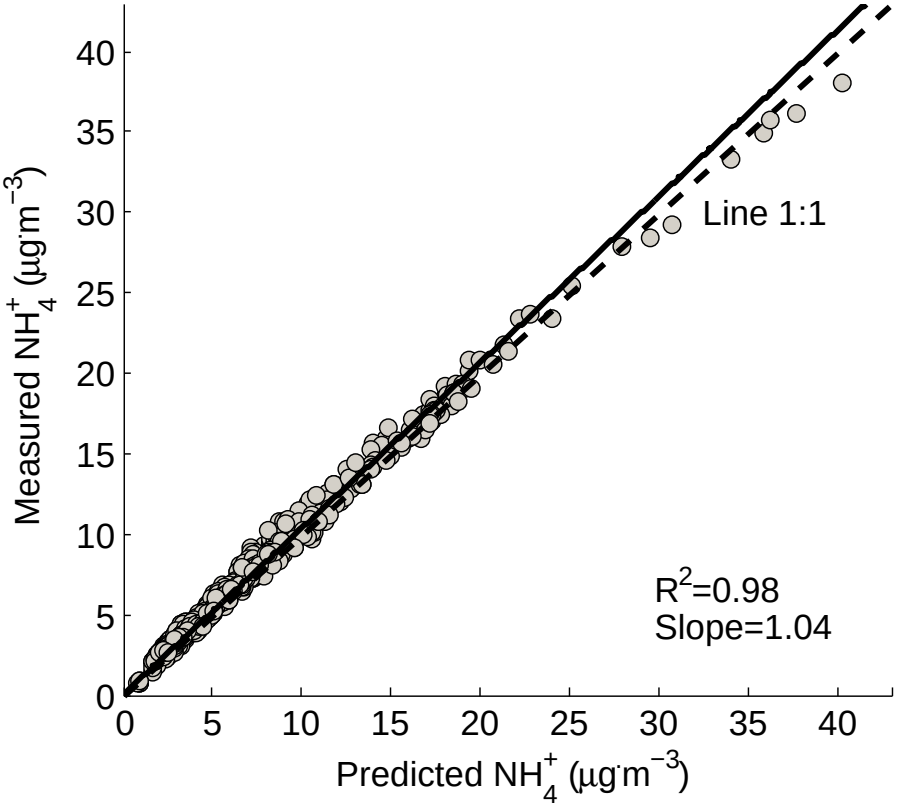

Figure 5. Measured and predicted mass concentration of ammonium. The predicted mass concentration of ammonium ($NH^+_{4\,predicted}$) is calculated by Eq. (4). The solid black line represents the linear least square regression.

ACPD
15, 2853–2904, 2015

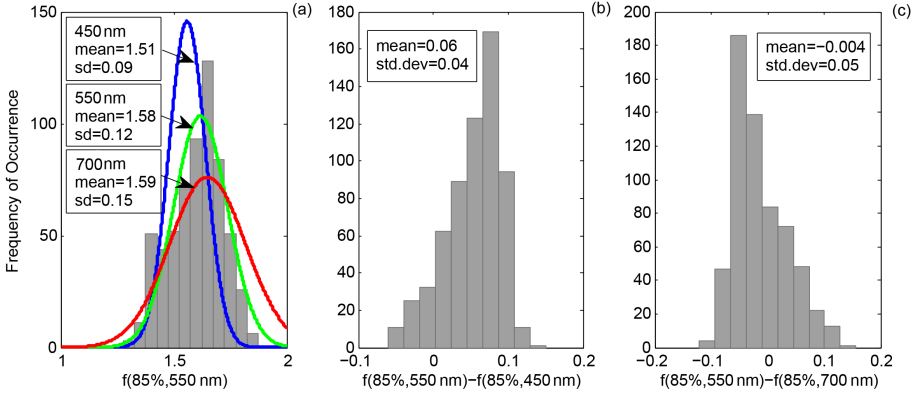

Figure 6. Histograms of **(a)** $f(85\%, 550\,\text{nm})$ overlaid with the Gaussian curves based on the statistics for $f(85\%, 450\,\text{nm})$, $f(85\%, 550\,\text{nm})$, and $f(85\%, 700\,\text{nm})$; **(b)** Frequency of occurrence of $f(85\%, 550\,\text{nm}) - f(85\%, 450\,\text{nm})$ and **(c)** $f(85\%, 550\,\text{nm}) - f(85\%, 700\,\text{nm})$.

ACPD
15, 2853–2904, 2015

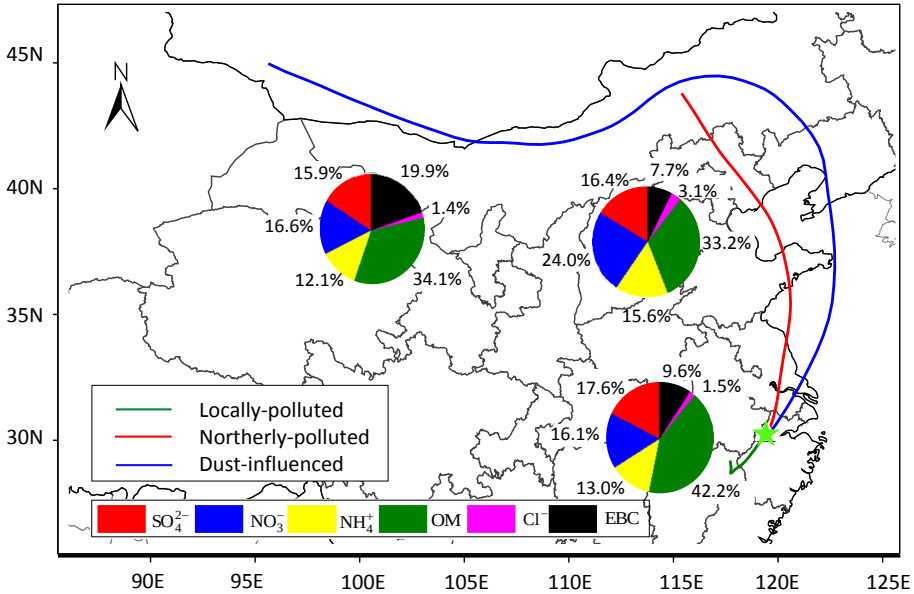

Figure 7. 72 h back trajectories of locally-polluted period, northerly-polluted period and dust-influenced period, together with the mean mass fraction of submicron chemical compositions (SO_4^{2-}, NO_3^-, NH_4^+, OM and Cl^-) measured by AMS and EBC in PM_{10} measured by MAAP.

ACPD
15, 2853–2904, 2015

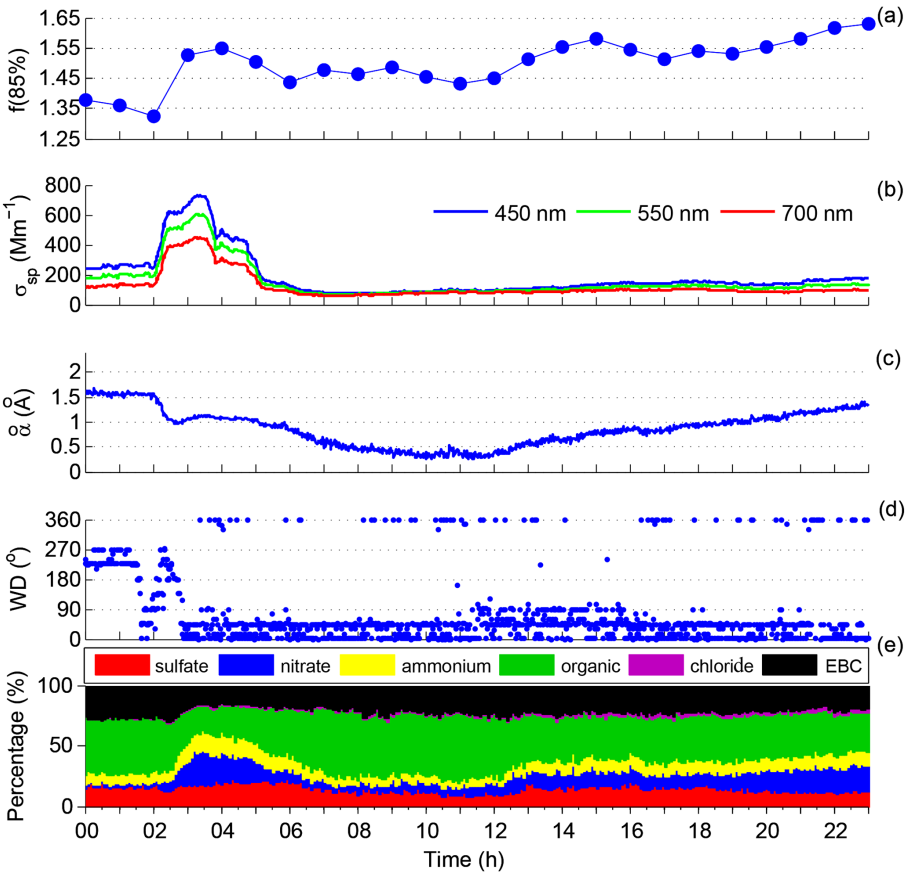

Figure 8. Parameters in episode influenced by dust on 10 March 2013 at LinAn **(a)** scattering enhancement factor at 85 % RH; **(b)** scattering coefficients at 3 wavelengths; **(c)** Ångström exponent; **(d)** wind direction; **(e)** mass percentages of chemical species measured by AMS and MAAP.

ACPD
15, 2853–2904, 2015

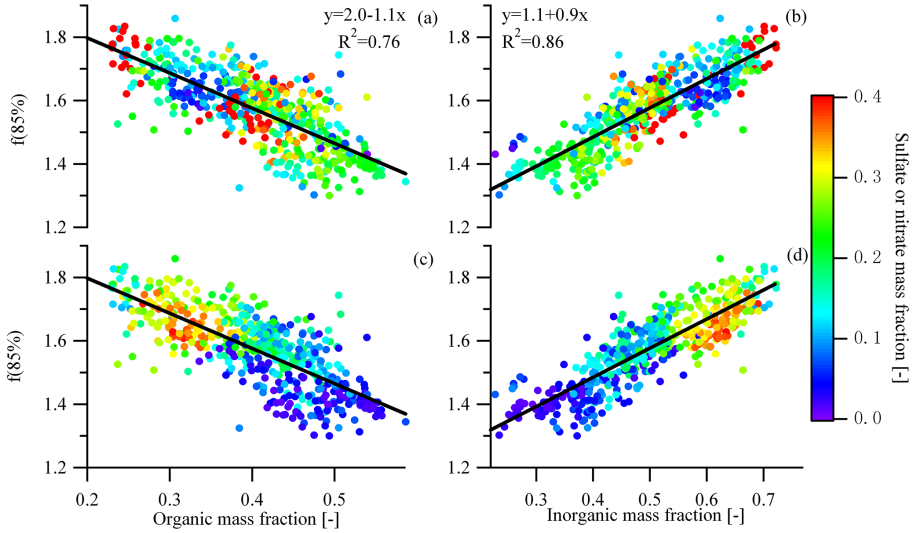

Figure 9. Scattering enhancement factor $f(85\%)$ vs. organic mass fraction and inorganic mass fraction measured by AMS and MAAP: **(a, b)** $f(85\%)$ vs. organic mass and inorganic mass fraction colored by sulfate mass fraction, respectively; **(c, d)** $f(85\%)$ vs. organic mass fraction and inorganic mass fraction colored by nitrate mass fraction, respectively. Solid black lines represent the linear least square regression.

ACPD
15, 2853–2904, 2015

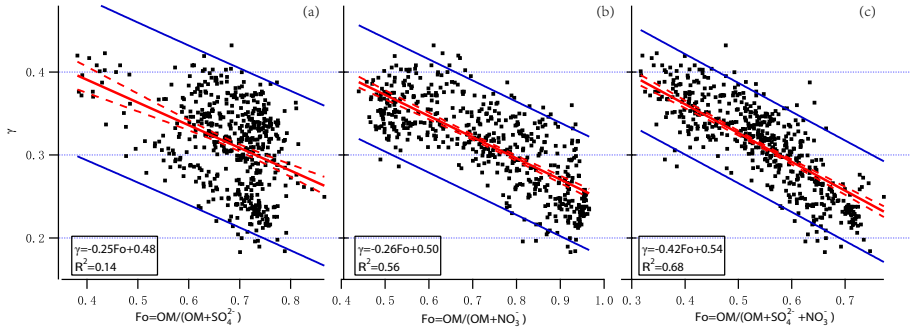

Figure 10. Scatter plots of γ vs. Fo **(a)** Fo = OM/(OM + SO_4^{2-}), **(b)** Fo = OM/(OM + NO_3^-) and **(c)** Fo = OM/(OM + SO_4^{2-} + NO_3^-). Solid red lines represent the linear fit, dashed red lines show the 95 % confidence level for the fit, and solid blue lines show the 95 % prediction bands.

ACPD
15, 2853–2904, 2015

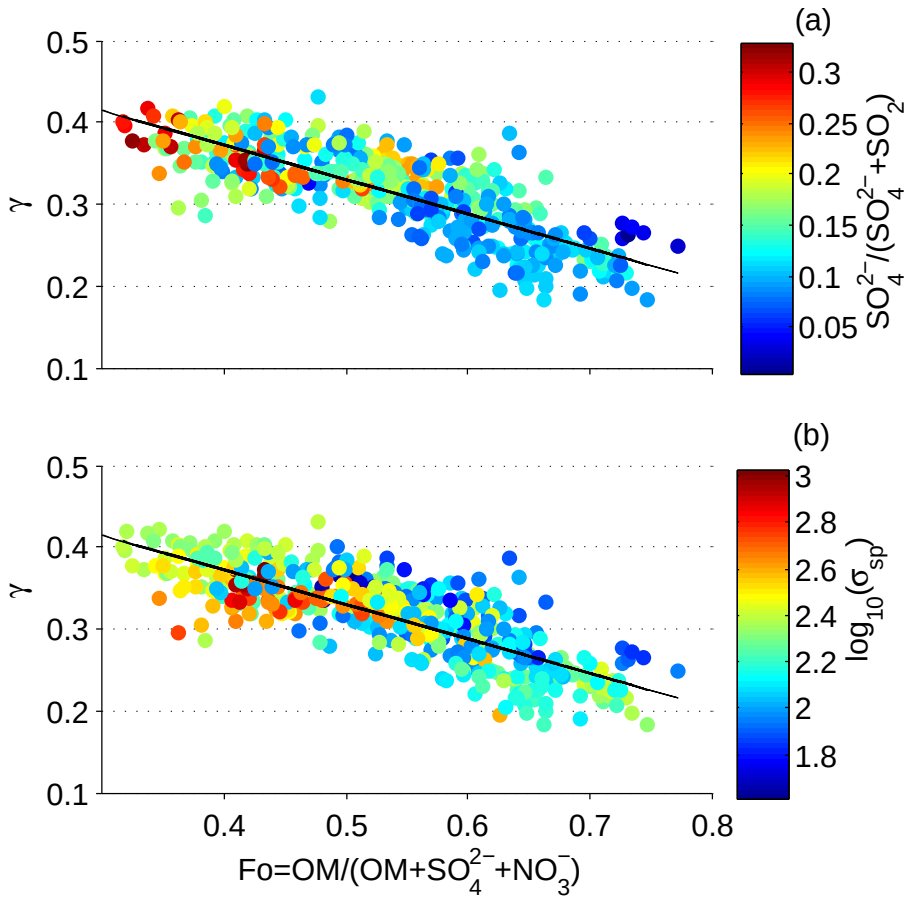

Figure 11. γ vs. Fo = OM/(OM + SO_4^{2-} + NO_3^-) colored by **(a)** $SO_4^{2-}/(SO_4^{2-} + SO_2)$ molar ratio and **(b)** $\log_{10}(\sigma_{sp})$.

ACPD
15, 2853–2904, 2015

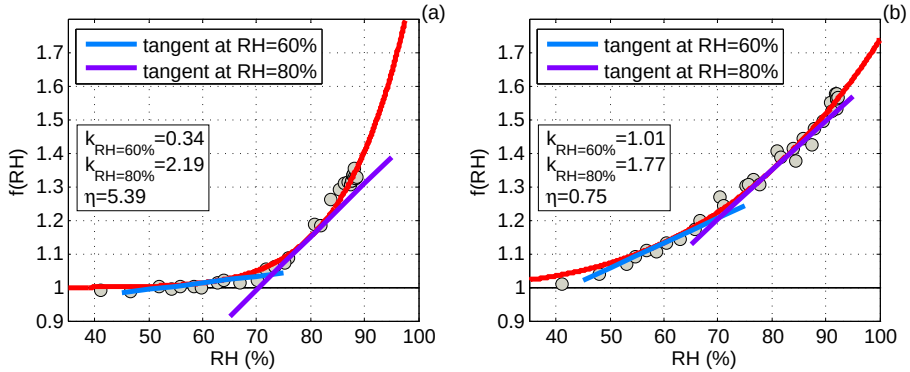

Figure 12. Two distinct examples showing different growth patterns and the corresponding η. **(a)** 8 March 2013 18 h f(RH) increase slowly at low RH (usually < 70 %) and then increase more steeply, thus η is big; **(b)** 10 March 2013 21 h increase with nearly constant speed and η is small. $k_{\mathrm{RH=60\,\%}}$ and $k_{\mathrm{RH=80\,\%}}$ represent the derivatives at 60 and 80 % RH, respectively.

ACPD
15, 2853–2904, 2015

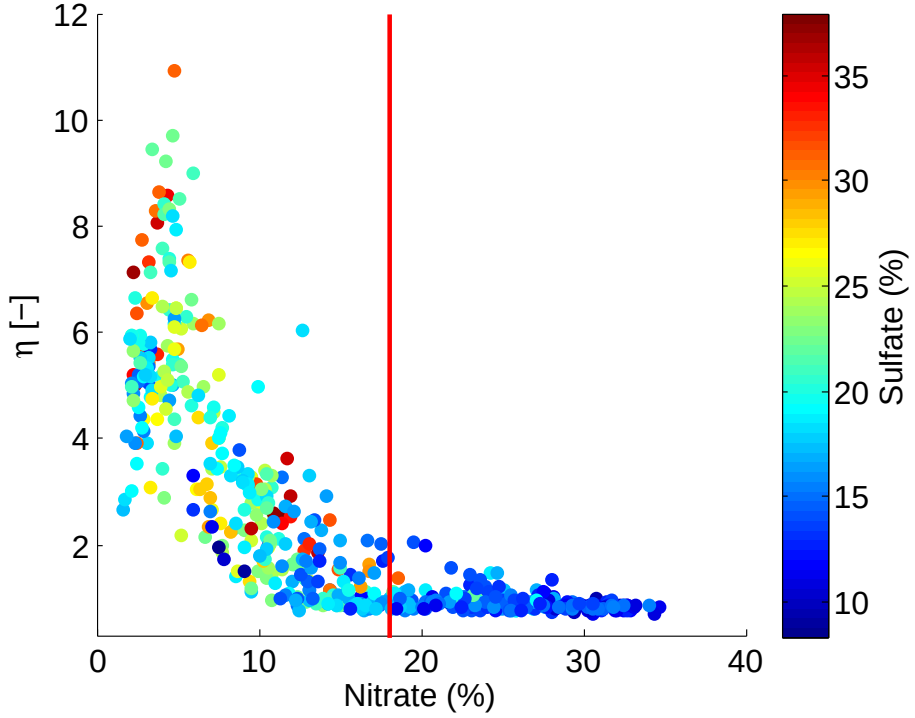

Figure 13. Scatter plot of η and the mass percentage of nitrate, colored by the mass percentage of sulfate.

ACPD
15, 2853–2904, 2015

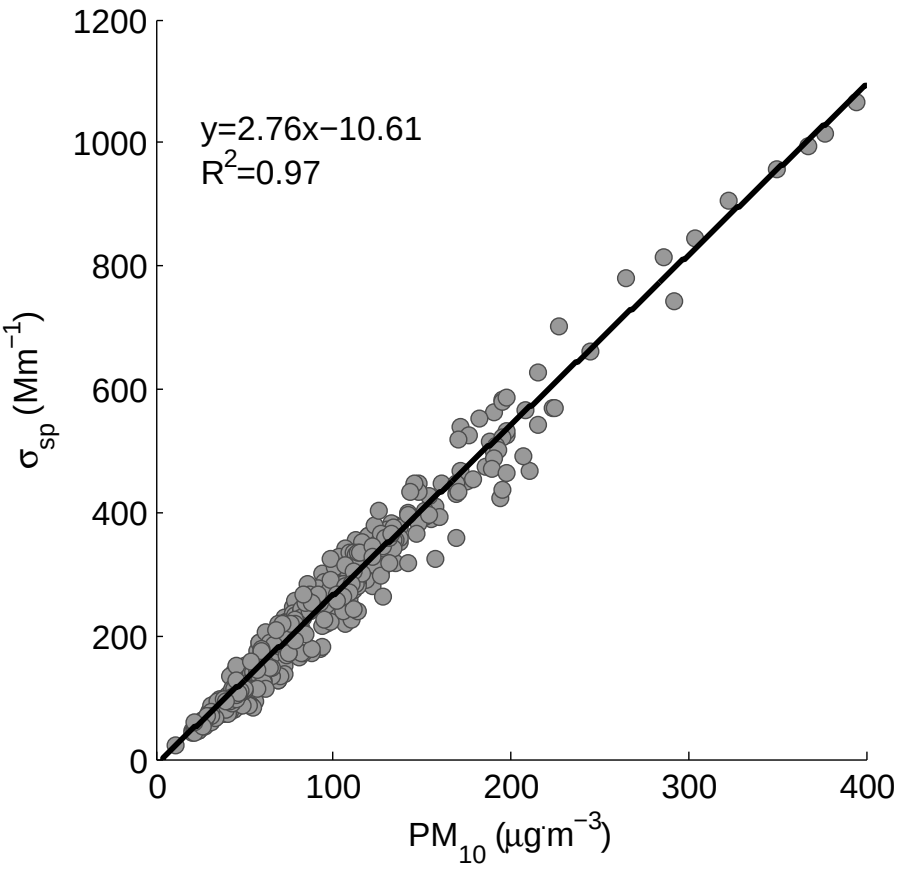

Figure 14. Linear regression of scattering coefficients (σ_{sp}) and PM_{10} mass concentration.

ACPD
15, 2853–2904, 2015